Tracing isotope precipitation patterns across Mexico

Ricardo Sánchez-Murillo[1*], Luis González-Hita[2], Miguel A. Mejía-González[2], Blanca Carteño-Martinez[2], Juan C. Aparicio-González[2], Dustin Mañón-Flores[2], Lucía Ortega[3], Milica Stojanovic[4], Raquel Nieto[4], and Luis Gimeno[4].

[1]Department of Earth and Environmental Sciences, University of Texas, Arlington, TX, 76019, USA
[2]Department of Hydrology, Mexican Institute of Water Technology, Mexico
[3]International Atomic Energy Agency, Isotope Hydrology Section, Vienna International Center, Vienna, Austria
[4]Centro de Investigación Mariña, Universidade de Vigo, Environmental Physics Laboratory (EPhysLab), Ourense, Spain.

***Corresponding author:**

Email: ricardo.sanchezmurrillo@uta.edu; https://orcid.org/0000-0001-8721-8093

lghita@tlaloc.imta.mx
mamejia@tlaloc.imta.mx
blanca_carteno@tlaloc.imta.mx
juan_aparicio@tlaloc.imta.mx
dustin@tlaloc.imta.mx
l.ortega@iaea.org
milica.s90@hotmail.com
rnieto@uvigo.es
l.gimeno@uvigo.es

LGH and MAMG conceived the experimental design. BCM and JCAG conducted the analytical isotopic analysis. DMF collaborated with precipitation sampling and data analysis. RSM prepared the initial draft. RSM and LO contributed to the temporal and spatial isotope assessments. MS, RN, and LG provided the moisture source-sink analysis. All authors contributed equally to drafting, revising, and preparing the final version of this manuscript.

This manuscript is a preprint under the peer-review process in PlosWater Journal.

Abstract

Mexico encompasses a large spectrum of landscapes with topographic, geographic, and climatic factors interacting in a complex ecohydrological setting. For decades, isotope hydrogeological tools have been applied in Mexico using short-term or seasonal local meteoric water lines as valid input functions. Yet, a systematic evaluation of meteoric isotope characteristics is still lacking. Here we report on the spatial and temporal isotope variations of 21 precipitation monitoring stations across Mexico. Our database includes 608 monthly samples collected from 2018 to 2021 over four regions (between 5 and 2,365 m asl): the Pacific coast, the Gulf of Mexico/Caribbean Sea region, and the Central and Northern Plateaus. Precipitation $\delta^{18}O$ seasonality from the dry (winter) to the wet season (summer) was characterized by a notable W-shaped variability. Monthly precipitation amounts and $\delta^{18}O$ compositions exhibited poor to strong linear regressions (*Adj.* r^2<0.01 to 0.75), with inverse (positive) relationships over the northern monsoon-affected region. Low *d*-excess (5.1 to 9.7‰) corresponded with greater terrestrial moisture contributions (20.5%) over the arid northern regions. Moisture inputs from the Gulf of Mexico/Caribbean Sea and the Pacific Ocean were associated with near-equilibrium or greater *d*-excess values (8.8 to 14.3‰), respectively. The best-fit linear models for $\delta^{18}O$ (*Adj.* r^2=0.85) and δ^2H (*Adj.* r^2=0.88) were determined on topographic and geographical predictors, resulting in an updated high-resolution precipitation isoscape (100 m^2 grid) for Mexico. Orographic barriers (-2.10‰ in $\delta^{18}O$/km) coupled with the interaction of tropical cyclones and cold fronts, the evolution of the North American Monsoon system, and the passage of easterly trade winds play a remarkable role in controlling the spatial isotope rainfall variability. Our findings provide a robust baseline for ecohydrological, climatic, forensic, archeological, and paleoclimate studies in North America.

Keywords: Mexico; stable isotopes; precipitation; moisture sources; isoscapes.

1. Introduction

Historically, the use of water isotopes (δ^2H, δ^{18}O) in hydrogeological studies has been site-specific across Mexico, where 1-2 years or even seasonal local meteoric water lines (LMWLs) have often been used as valid input functions in central Mexico [1-6], in the northern arid landscapes [7-9], and in the southern coastal wet regions [10-12] to underpin rainfall to groundwater and surface water connectivity.

For decades, however, most studies have relied on data archives of two stations from the Global Network of Isotopes in Precipitation [13] operated in Mexico from 1962 to 1988, one in the city of Chihuahua (northern arid region) and a second one in the city of Veracruz (southeastern wet region) [14]. The latter represents a relatively low number of monitoring stations for such a large and heterogeneous country, with abundant rain in the south and scarce in the north, with rain forests but also with vast deserts, tropical and mid-latitude climates, with coastlines facing the Pacific Ocean, the Gulf of Mexico and the Gulf of California, and the Caribbean Sea, and with an enormous plateau bounded by two mountain ranges where ice caps are still present [15]. Similarly, Mexico is affected by multiple climatic features, such as the influence of cold fronts [16], atmospheric rivers [17], easterly waves [18], tropical cyclones [19], and northerly trade winds. All these topographic, geographic, and weather characteristics are represented in a large spectrum of climatic regions across Mexico [20].

Although catchment to basin-scale studies are numerous across Mexico, only four isotopic geospatial efforts [21] have been reported. Wassenaar et al. [22] interpolated groundwater isotopic values based on the premise that the water isotope ratios of shallow groundwater (N=234 at near 50 km latitudinal spacing) can be used as a proxy of the stable isotopic composition of long-term seasonally weighted precipitation. This product was later used to construct a feather hydrogen isoscape (i.e., migrant bird isoscape based on feather deuterium compositions) for Mexico [23]. Ammer et al. [24] used 158 tap water samples from 51 towns and cities collected throughout Mexico for six weeks from June to July 2018 to infer the region of origin of unidentified border crossers between Mexico and the United States. Lately, Fan et al. [25] studied $\delta^{18}O$, $\delta^{2}H$, and *d*-excess (N=205) in surface water collected in wet and dry seasons from the west to the east coast of Mexico between 22°N and 26°N to understand the controlling factors of isotopic patterns and lapse rates. Nevertheless, a systematic and regional evaluation of isotope meteoric characteristics across Mexico is still lacking.

Here we report on the spatial and temporal isotope variations of 21 precipitation monitoring stations across different physiographic units of Mexico (https://en.www.inegi.org.mx/temas/fisiografia/). These stations are part of the National Network of Isotopes in Precipitation (known as RENIP) operated by the Department of Hydrology of the Mexican Institute of Water Technology (IMTA). Our database includes 608 monthly samples collected from 2018 to 2021 over four regions: the Pacific coast (PC), the Gulf of Mexico and the Caribbean Sea coast (GCS), and the Central (CP) and Northern Plateaus (NP). Monitoring sites are located between 5 and 2,365 m asl with distinct topographic, geographic, and weather characteristics. The main goal of our study is to evaluate the spatial and temporal isotopic variability in precipitation across Mexico. This will be complemented with an atmospheric analysis of the trajectories that reach the region using the FLEXPART Lagrangian model [as in 26]. This analysis differentiates between the monthly contribution of moisture sources from oceanic and terrestrial domains. Emergent relationships resulted in updated precipitation isoscapes ($\delta^{18}O$, $\delta^{2}H$, *d*-excess) for Mexico. Our spatial and temporal analysis should also serve as a baseline for ecohydrological, climatic, forensic, archeological, and paleoclimate studies in north America.

2. Topographic features

Mexico is part of the northern hemisphere, ranging from 14°30'N to 32°43'N (Fig. 1). A fraction of the territory is located within the subtropical zone (north of the Tropic of Cancer), while the southern portion is part of the tropics [15]. A notable orographic feature is an enormous plateau called the Mexican Plateau, bounded to the west by the Sierra Madre Occidental and to the east by the Sierra Madre Oriental [27]. This plateau intercepts the westerly winds that are characteristic of the middle latitudes. Due to their low humidity, these winds produce the characteristic dryness that prevails during the cold season of the year.

The Sierra Madre Oriental is a mountain range approximately 1,350 kilometers long and 80 to 100 km wide, extending from the south of the Rio Bravo, parallel to the Gulf of Mexico, to the Neovolcanic Axis, which separates North America from Central America [28]. Headwater elevation oscillates between 2,000 and 3,000 m asl in this mountain range. Under favorable synoptic-scale flow [29], cold winter surges propagate from North America deep into the tropics bounded by the eastern side of the Sierra Madre Oriental [30-32]. The Isthmus of Tehuantepec, located in southeastern Mexico, is a narrow region that separates the Gulf of Mexico from the Pacific Ocean. The Sierra Madre del Sur range has an average altitude of 2,000 m asl, but on the Isthmus of Tehuantepec, the elevation drops to 250 m, forming a gap approximately 40 km wide and 220 km long, known as ‘Paso Chivela’.’ It is through this gap that cold fronts sometimes leak into the Pacific Ocean.

Another important mountain range of the country is the Sierra Madre Occidental, which extends over 1,400 km from the northern border to the central part of the country, bordering the Pacific Ocean [28]. With an average altitude of 2,000 m asl, it reaches maximum altitudes of 3,300 m in the state of Chihuahua [28]. When atmospheric rivers from the western Pacific Ocean influence the northwestern region, water vapor rises over the Sierra Madre Occidental, generating abundant precipitation [33-34].

The main physiographic component of central Mexico is the Mesa Central or Central Plateau, a region that encompasses the Trans-Mexican Volcanic Belt. It limits to the south with the Balsas depression, to the east with the Sierra Madre Oriental, to the west with the Sierra Madre Occidental, and to the north with Zacatecas. This region comprises several volcanoes such as Pico de Orizaba (5,363 m asl), Popocatepetl (5,426 m asl), Nevado de Toluca (4,690 m asl), Colima (4,330 m asl), and Cofre de Perote (4,282 m asl). The high relief is one of the main factors influencing the distribution of precipitation in this region, from values greater than 2,500 mm (windward) to 500 mm (leeward) [35] (Fig. 1).

The southeast region includes the Yucatan Peninsula with an elevation below 300 m asl [15] surrounded by the Gulf of Mexico and the Tabasqueña lowlands. On the Pacific slope of this region, there is a low area of 600 to 900 m asl, and to the north of this depression, the Central Plateau of Chiapas runs to the coastal plain of the Gulf of Mexico [15].

3. Climatic and meteorological characteristics

Among the climatic and meteorological components that influence the annual precipitation cycle in Mexico are the North American high (NAH), the North Atlantic subtropical high (NASH), the North American Monsoon System (NAMS), cold fronts, atmospheric rivers, easterly waves, and tropical cyclones. The NAH is a center of high atmospheric pressure located across most of North America during the boreal winter. Cold and dry air masses flow from the NAH, causing cold fronts in the region (September to May) [16]. Depending on the atmospheric conditions, the convergence of the cold fronts with moisture advected from the Gulf of Mexico and the Pacific Ocean could result in rainfall events.

High vertically integrated water vapor bands are formed at the convergence zone of the cold fronts and the warm conveyor belt of extratropical systems [36]. Such moisture bands, called atmospheric rivers (Ars), are formed over the oceans, and are typically associated with extratropical cyclones, covering long (thousands of kilometers) and narrow (hundreds of kilometers) transient water vapor corridors [37]. The influence of ARs is relevant in northwestern Mexico, whereby rainfall is produced via this mechanism during the winter season [33-34].

During the summer season, the air over the continent warms up more than the air over the ocean, producing a pressure gradient between the continent (low pressure) and the ocean (high pressure). The pressure gradient induces wind currents that transport moisture from the ocean to the continent. The moisture warmed by the terrestrial heat flux is lifted in a strong upward air motion to high altitudes, producing convective rain (i.e., NAMS) [38]. Convective rain provides a substantial fraction of the total annual precipitation in northwestern Mexico (60%-80%) [39].

The NASH is a center of high atmospheric pressure in the Atlantic Ocean, located around 30°N, which varies in extension and intensity during the year [40]. During the winter, it weakens and contracts, and by early May, it begins to strengthen and expand, which continues until the end of July [41]. The winds produced by the NASH, called northerly trade winds, transport moisture from the Caribbean Sea and the Gulf of Mexico towards Central America, Mexico, and the southeastern United States [40].

During the summer, the northerly trade winds converge with the southerly trade winds in the tropical portion of Mexico [42], generating updrafts that condense the moisture and produce abundant rainfall [43]. Another important source of precipitation in the tropics of Mexico is the easterly waves (Ews). They are inverted troughs of low pressure, propagating from east to west (i.e., across the Atlantic Ocean and originated near the western coast of Africa) from May to November, with lengths of 2,000-2,500 km, and within latitudes 5^{o} and 20^{o} N. Easterly waves are highly convective systems, producing at least 20% of southern Mexico's precipitation [44]. In addition, Mexico is located between the cyclogenetic regions of the northern Atlantic Ocean and the northeastern Pacific Ocean, receiving abundant rains from tropical cyclones (TCs) during the summer. On average, five tropical cyclones enter the national territory yearly [45]. Mexico receives up to 20% of its total annual rainfall from TCs [19].

4. Materials and Methods

4.1 Data collection

Monthly precipitation samples (N=608) in 21 stations (Fig. 1) were collected from 2018 to 2021 using a passive precipitation collector (RS2 Palmex, Croatia) [46]. This type of collector prevents secondary evaporation by using the principle of minimum exposure of the collected water surface area to the atmosphere [See 46 for more details]. Samples were filtered using cellulose membranes with 0.45 µm pore size, collected in 60 mL high-density polyethylene bottles with conic and poly seal inserts, filled with no headspace, and stored at 5°C until analysis. Rainfall amounts (mm) were calculated based on the volume of rain collected and the funnel's diameter. Collectors were installed at the facilities of the National Meteorological Service of the National Water Commission. The network was designed to cover all 15 and 13 physiographic provinces and precipitation zones, respectively (Fig. 1).

Figure 1: Map of Mexico including mean annual precipitation (in mm) (1981-2019; based on CHIRPS data) [47], isotope monitoring sites (monthly sampling frequency; pink circles, dotted), and physiographic regions (dashed-line polygons; obtained from https://en.www.inegi.org.mx/temas/fisiografia/). The number of monitoring sites per physiographic region ranged from 1 to 5.

4.2. Stable isotopes analysis

Stable isotope analyses were conducted at the Isotope Hydrology Laboratory of the Mexican Institute of Water Technology (IMTA), using laser water isotope analyzers Picarro L2110-*i* and Los Gatos Research LWIA-45EP (Supplementary Table S1; available from Hydroshare at http://www.hydroshare.org/resource/909aaa5edf1040b6a6244a0ca7f58890 [48]. The long-term analytical precision was ±0.5‰ for δ^2H and ±0.13‰ for $\delta^{18}O$. The secondary standards were Popocatepetl Volcano Water, PVW (δ^2H= - 81.4‰, $\delta^{18}O$= - 11.79‰), Laguna Verde Water, LVW (δ^2H=+17.1‰, $\delta^{18}O$=+3.38‰), and Playa del Carmen Well Water, PCWW (δ^2H=-28‰, $\delta^{18}O$=-4.8‰). PVW and LVW standards were used to normalize the results to the VSMOW2-SLAP2 scale, while PCWW was used as a quality control and drift control standard. A least-squares regression of the isotope data was used to obtain the local meteoric water lines. Deuterium excess (*d*-ex=$\delta^2H-8*\delta^{18}O$) was used to evaluate secondary evaporation and moisture recycling [49]. Precipitation-weighted (δ_w) values were calculated as $\delta_w=\Sigma P_i*\delta_i/P_T$, where P_i is the precipitation amount, δ_i is the isotope composition (δ^2H or $\delta^{18}O$) of the sample, and P_T is the total precipitation amount [50]. Precipitation-weighted *d*-excess values were also estimated.

4.3. Isoscape modeling and statistical analysis

Isoscapes (100 m^2 grid resolution) were generated using precipitation-weighted $\delta^{18}O$ and δ^2H data (Table 1). The best-fit regressions were determined on topographic (i.e., elevation-Elv) and geographical (i.e., latitude-Lat and longitude-long) regressors following similar isoscape procedures [51, 52]. The regression equations used as suitable predictions for the annual mean $\delta^{18}O$ and δ^2H in Mexico are:

$\delta^{18}O=0.206\cdot Long+0.299\cdot Lat-0.00172\cdot Elv+8.766$ (*Adj.* r^2=0.85; *p*-value <0.001; RMSE=0.690) (Eq.1)

$\delta^2H=1.680\cdot Long+2.209\cdot Lat-0.0142\cdot Elv+88.98$ (*Adj.* r^2=0.88; *p*-value <0.001; RMSE=37.75) (Eq.2)

All linear regressions and statistical diagnostics were computed using R [53]. Raster calculations were performed in ArcGIS 10.8.1 (ESRI, USA) using a 10m digital elevation model, and latitude/longitude rasters. Mean annual $\delta^{18}O$ and $\delta^{2}H$ (‰) predicted residuals were evaluated against a) the observed values and B) a global isoscape product [54, 55] (See Supplementary Table S2; available from Hydroshare at http://www.hydroshare.org/resource/909aaa5edf1040b6a6244a0ca7f58890) [48]. Open access base maps were obtained from ESRI (world ocean base; https://www.arcgis.com/home/item.html?id=1e126e7520f9466c9ca28b8f28b5e500%2F) and Nature Earth (coastlines; https://www.naturalearthdata.com/downloads/110m-physical-vectors/).

4.4. Budyko framework

To facilitate the understanding of regional water partitioning differences and similarities across the monitoring regions, we computed a representative Budyko framework [56] for the main physiographic units across Mexico. We used regional actual and potential evapotranspiration values (AET and PET, respectively) and precipitation records (P) from previous studies [57]. The physiographic regions are also contextualized within the global Budyko curve (ω=2.6) [58,59].

4.5. Computation of monthly moisture sources contribution

The isotope monitoring stations were grouped in six moisture sink regions (i.e., Central and Northern Plateaus, North and South Pacific, and Northern and Southern Gulf), based on the precipitation patterns (Fig. 1) and previous moisture source tracking studies over Mexico and the southwestern USA [60-63]. Moisture sinks refer to air parcels that lose humidity through, for instance, precipitation processes.

Supplementary Figure S1 shows the experimental regional setting for the FLEXPART calculations. The air masses residing over each of the six study regions were tracked backward in time using the FLEXible PARTicle dispersion model (FLEXPART) v9.0 [64,66] and by moving the particles (atmospheric air masses) considering the optimum integration time was found in to be 5 days prior to the time that the precipitation event ended [67]. In this experiment, FLEXPART computes trajectories of nearly 2 million particles with a horizontal resolution of 0.25º, along with the changes of specific humidity (dq) which is calculated on each parcel, based on the budget of the evaporation (e) minus precipitation (p). ERA-Interim wind fields are used to model the positions of the particles and thus the air masses advection. Integrating dq on the vertical column with 61 vertical levels from the surface to 0.1 hPa permits estimating the surface freshwater balance [65]. Along the trajectories, the moisture gained by air masses was computed to determine the sources of moisture.

The sources were calculated by the net positive values of the evaporation minus precipitation budget (E-P>0; where evaporation exceeds precipitation) on the parcels along the vertical column. Four individual sources (i.e., terrestrial, the Pacific Ocean, the Gulf of Mexico, and the Caribbean Sea) were identified. Then, a forward-in-time analysis was performed to compute over each study region their contribution to precipitation, which is assumed as the negative values on the budget of the evaporation minus precipitation (E-P<0; where precipitation exceeds evaporation). This approach has been widely utilized in several previous studies following the methodology designed by [64, 66, 68] for several regions of the world [67, 69,70], confirming its reliability for the source-sinks of atmospheric moisture assessment, and its implication in the hydrological cycle at local, regional, and global scales.

5. Results

5.1. Hydrological framework across Mexico

Moisture recycling and sub-cloud evaporation play a relevant regional and local role in the configuration of meteoric water lines worldwide [71,72]. Water partitioning, and in particular, the transpiration flux is of interest since it accounts for between 60-90% of global terrestrial evapotranspiration [73,74]. Figure 2 shows a representative Budyko framework for the main physiographic regions of Mexico. The Chiapas ranges, the southern Gulf coastal lowlands, and the southern Sierra Madre are represented by an aridity ratio<1, meaning precipitation exceeds the evaporative demand (PET), representing energy-limited areas with substantial runoff [75]. This is typical of humid coastal and tropical high-elevation mountains [76]. Regions such as the northern Gulf lowlands, eastern and western Sierra Madre, and the Neovolcanic axis exhibited an aridity ratio between 1 and 2, with trends towards less runoff and more arid conditions [77]. The Central Plateau is in a transitional Budyko space towards more arid conditions. Conversely, the northern lowlands and ranges, the Sonora and North America plains, the Pacific coast lowlands, and the Baja California peninsula denote a trend in the direction of arid regions with more evaporative demand (PET) than precipitation (>1), a common feature of low elevation landscapes in northern Mexico. These characteristics are further discussed in section 5.5. from a moisture source perspective.

Figure 2: Budyko dual-space framework for the main physiographic regions (color coded). The X axis is the ratio of potential evapotranspiration (PET) to precipitation (P) (dryness index), and the Y axis represents the actual evapotranspiration (ET) over P (evaporative index). The blue line shows the 'Budyko curve' defined by ω=2.6 [58, 59]. Grey solid lines define the energy and water limits.

5.2. Seasonal precipitation and isotopic patterns

Mexico exhibits a monsoonal climate, with a rainy season during the summer months (June-September) and a relatively dry season in winter (Fig. 3a; Table 1), with fluctuations linked to cold fronts, tropical cyclones (landfall and passages), monsoonal rainfall (e.g., NAMS), and easterly waves passages [78]. Along the GCS region and in less degree in the CP, monthly precipitation revealed a bimodal distribution with two maxima in June and September (Fig. 3a). During the summer (June-September), trade winds from the north (moisture from the Gulf of Mexico) and trade winds from the south (moisture from the Pacific Ocean) converge in the tropics of Mexico, generating abundant precipitation [43]. The GCS domain also received abundant precipitation in July-October due to the activation of the Atlantic hurricane season. Both regions experienced a precipitation decrease from November to April. In the PC region, precipitation increased from June to September due to the direct/indirect effect of tropical cyclones from the eastern Pacific Ocean and the activation of the NAMS. In the NP region, a precipitation maximum was observed between July and September, a region largely governed by the NAMS (60-80% of total annual precipitation) [79, 80].

Figure 3: Monthly box plots of (a) precipitation (mm), (b) $\delta^{18}O$ (‰), and (c) *d*-excess (‰) for all monitoring sites in the Central Plateau (CP), the Gulf of Mexico and the Caribbean Sea coast (GCS), the Northern Plateau (NP), and the Pacific coast (PC).

Table 1: Summary including site name, geographic location (latitude/longitude), elevation, arithmetic and precipitation-weighted (*w*-subscript) means ($\delta^{18}O$, $\delta^{2}H$, and *d*-excess), and region classification.

Site name	**Latitude (decimal degrees)**	**Longitude (decimal degrees)**	**Elevation (m asl)**	**$\delta^{18}O$ (‰)**	**$\delta^{2}H$ (‰)**	***d*-excess (‰)**	**$\delta^{18}O_w$ (‰)**	**$\delta^{2}H_w$ (‰)**	***d*-excess$_w$ (‰)**	**Slope**	**Region (acronym)**
Pachuca	20.0876	-98.7497	2,365	-8.37	-56.7	10.3	-10.82	-75.2	11.3	Leeward	Central Plateau (CP)
CDMX	19.4037	-99.1966	2,322	-7.30	-46.9	11.5	-9.20	-61.3	12.2	Leeward	Central Plateau (CP)
Tulancingo	20.0842	-98.3577	2,205	-6.83	-42.6	12.1	-10.32	-69.7	12.9	Leeward	Central Plateau (CP)
Queretaro	20.5634	-100.3694	1,820	-7.36	-49.5	9.4	-8.67	-58.9	10.5	Leeward	Central Plateau (CP)
Tuxtla Gutierrez	16.7629	-93.1474	577	-5.14	-30.6	10.5	-6.95	-44.6	11.0	windward /leeward	Gulf of Mexico and Caribbean Sea (GCS)
Monterrey	25.6824	-100.2717	494	-3.95	-17.3	14.3	-6.00	-34.0	13.9	windward	Gulf of Mexico and Caribbean Sea (GCS)
Cd. Victoria	23.7425	-99.1699	329	-3.26	-12.9	13.2	-4.53	-22.7	13.5	windward	Gulf of Mexico and Caribbean Sea (GCS)
Tapachula	14.8872	-92.2962	128	-4.13	-20.4	12.6	-5.60	-31.5	13.3	windward	Gulf of Mexico and Caribbean Sea (GCS)

Chetumal	18.5004	-88.3275	19	-2.79	-9.9	12.4	-4.26	-21.1	13.0	windward	Gulf of Mexico and Caribbean Sea (GCS)
Veracruz	19.1428	-96.1113	15	-3.12	-13.3	11.7	-4.30	-22.7	11.7	windward	Gulf of Mexico and Caribbean Sea (GCS)
Merida	20.9466	-89.6518	12	-2.85	-12.6	10.2	-4.36	-24.9	10.0	windward	Gulf of Mexico and Caribbean Sea (GCS)
Villahermosa	17.9809	-92.9213	5	-3.61	-16.4	12.5	-4.06	-20.0	12.5	windward	Gulf of Mexico and Caribbean Sea (GCS)
Durango	24.0614	-104.6004	1,882	-6.77	-49.1	5.1	-7.37	-54.9	4.1	Leeward	Northern Plateau (NP)
Chihuahua	28.6709	-106.0310	1,405	-7.32	-50.7	7.9	-6.30	-40.3	10.1	Leeward	Northern Plateau (NP)
Torreon	25.5201	-103.4161	1,124	-5.76	-40.5	5.6	-6.24	-40.1	9.8	Leeward	Northern Plateau (NP)
Piedras Negras	28.6836	-100.5489	251	-2.57	-12.0	8.6	-3.42	-17.1	10.3	Leeward	Northern Plateau (NP)
Hermosillo	29.0785	-110.9305	209	-6.07	-38.8	9.7	-6.39	-41.4	9.7	windward	Northern Plateau (NP)
Guadalajara	20.7066	-103.3926	1,568	-8.28	-55.4	10.8	-9.39	-62.2	12.9	windward	Pacific (PC)

Chilpancingo	17.5717	-99.5140	1,270	-6.57	-41.9	10.7	-8.77	-57.8	12.4	windward	Pacific (PC)
Culiacan	24.6351	-107.4411	30	-5.99	-37.4	10.5	-6.72	-41.1	12.7	windward	Pacific (PC)
Loreto	26.0116	-111.3492	6	-6.09	-40.0	8.8	-6.81	-45.2	9.3	windward	Pacific (PC)

Precipitation $\delta^{18}O$ (similar patterns are observed in $\delta^{2}H$) seasonality across Mexico from the dry to the wet season was characterized by a notable W-shaped variability (Fig. 3b). This pattern is similar to the observed intra-seasonal variability of Central American rainfall, which typically results in two or three depletions during the wet season (boreal summer) and more enriched values during the strongest trade winds period (boreal winter) [51]. Across the GCS domain (windward slope), median $\delta^{18}O$ values varied between -7.0 (June) to 0.0‰ (Dec-Apr) with a more attenuated W-trend as a result of the incipient orographic distillation (proximity to the coast) [22] (Fig. 3b). During the winter season, median $\delta^{18}O$ values are nearly uniform within the GCS domain (ranging from -2.5 to -1.0 ‰). In contrast, strong orographic distillation within central Mexico is denoted by the most depleted $\delta^{18}O$ compositions (up to -20‰) during the summer (wet season) (Fig. 3b). The Pacific domain was characterized by a similar trend with median values near -10‰ in $\delta^{18}O$. In the NP, depleted values were observed during the winter season (Jan-Feb), whereas more enriched values occurred during the influence of the NAMS (June-September) (Fig. 3b) [81, 82].

Consistently, the lowest *d*-excess values were reported in northern Mexico (Fig. 3c). Across this arid region (Fig. 2; water-limited), a larger temperature seasonality, low relative humidity, and small rainfall events resulted in *d*-excess values as low as -12‰. In this region, February-March (dry season; cold fronts) and September (monsoon) exhibited the largest *d*-excess variability (from -10 up to 20‰) among all sites. The PC sites also resulted in low *d*-excess values but with a remarkably reduced variability (Fig. 3c), indicating a potential constant moisture source from the Pacific Ocean. In general, the wet season (boreal summer) was characterized by a nearly uniform *d*-excess around 10‰ (CP, PC, and GCS domains) and greater values and variability during the winter season (Fig. 3c).

5.3. Regional precipitation amount and isotope relationships

Recent studies across tropical and subtropical regions have shown that condensation levels, weather types, and stratiform fractions better predict the precipitation isotope composition than the classical precipitation amount [83-86]. This can be observed in the inherent complexity of monthly precipitation relationships across Mexico (Fig. 4). For example, in northern Mexico, positive regressions between precipitation amount and $\delta^{18}O$ are a characteristic feature of NAMS-dominated regions, ranging from +0.4 up to +2.3‰ per 100 mm of precipitation (Fig. 4). In low-elevation PC sites, poor regressions were reported (-0.01 to +0.2‰ per 100 mm; r^2=*0.01-0.23*), except for the Chilpancingo site (-0.8‰ per 100 mm; r^2=0.69), located in the southern Pacific coast and above 1,000 m asl. A tropical cyclone bias was also detected in the north Pacific lowland stations (e.g., Culiacan and Loreto). The strongest amount effect was exhibited in central Mexico (-1.0 to -2.2‰ per 100 mm; r^2=0.31-0.70) and the GCS domain (-0.4 to -1.1‰ per 100 mm; r^2=0.55-0.75). Monterrey (-0.4‰ per 100 mm; r^2=0.15) and Villahermosa (-0.2‰ per 100 mm; r^2=0.01) sites resulted in weak regressions.

The strongest isotope lapse rate was reported within the windward slope (over the Sierra Madre Oriental) of the Gulf of Mexico and the Caribbean Sea, -2.6‰ in $\delta^{18}O$ per km of elevation (*Adj.* r^2=0.58, p=0.030) (Fig. 5). This lapse rate agrees with earlier reported values in rainfall, groundwater, and surface water within the Caribbean Sea slope of Costa Rica (windward over the central Cordillera), -2.5‰ in $\delta^{18}O$ per km of elevation [55]. In the CP, the isotopic lapse rate is weaker, -0.90‰ in

$\delta^{18}O$ per km of elevation (*Adj.* r^2=0.11, p=0.657). In the PC and NP, moderate isotopic lapse rates ranged from -1.11‰ (*Adj.* r^2=0.73, p=0.141) to -1.74‰ (*Adj.* r^2=0.45, p=0.211) in $\delta^{18}O$ per km of elevation, respectively. The nationwide isotopic lapse rate (including monitoring sites influenced by TCs; Loreto, Culiacan, and Hermosillo) corresponds to -1.75‰ in $\delta^{18}O$/km (*Adj.* r^2=0.65, p-value <0.001). The direct influence of TCs passages and landfalls across the Pacific coast resulted in depleted monthly compositions in low-elevation coastal sites during the study period. The precipitation-weighted isotope lapse rate (including all sites) resulted in a similar slope -2.10‰ in $\delta^{18}O$/km (*Adj.*r^2=0.72, p-value <0.001). The lapse rate obtained in the isoscape modeling resulted in -1.72 $\delta^{18}O$/km. No significant trend was found between d-excess and elevation (Fig. 5). Overall, monitoring sites along the Gulf of Mexico and Caribbean Sea basins resulted in greater *d*-excess values, whereas high-elevation sites in the northern plateau exhibited lower *d*-excess values.

Figure 4: Monthly precipitation amount and $\delta^{18}O$ (‰) relationship per site across Mexico. Regions are color-coded.

Figure 5: Elevation (m asl), $\delta^{18}O$ (‰), and *d*-excess (‰) relationship across Mexico. Regional isotopic lapse rates are color-coded and ranged from -0.90 to -2.60 ‰ in $\delta^{18}O$ per km.

5.4. Regional meteoric water lines

Figure 6 shows dual isotope diagrams for all monitoring sites. The arid conditions in the NP (Fig. 2) resulted in the lowest intercepts and slopes, ranging from 0.92 to 1.60 and from 5.1 to 7.4, respectively. Overall, the rainfall isotopic composition within the NP agrees with previous LMWLs described for Chihuahua (northern Mexico), Tucson, Arizona [81, 82], and the Sonora River basin [8]. In the GCS domain, isotope compositions were right-skewed toward more enriched compositions. However, sporadic depleted monthly $\delta^{18}O$ compositions (< -10‰) were reported in Monterrey, Villahermosa, and Tuxtla Gutierrez. Within this region, LMWLs are characterized by slopes close to the GMWL and relatively high intercepts (11.2 to 14.0). The latter is a common feature of monitoring sites across the Caribbean coast of Central America [51, 55]. Intercepts below the global mean (10‰) were reported in Tuxtla Gutierrez (9.4) and Merida (8.7). In the CP, LMWLs represent equilibrium conditions with slopes (7.6 to 8.0) and intercepts (9.9 to 10.2) near the GMWL. In this region, Queretaro exhibited a relatively lower intercept (6.8). Commonly, the CP received depleted precipitation events below -15‰ in $\delta^{18}O$ because of strong orographic effects during convective summer precipitation events. The PC domain is characterized by moderate slopes (7.2 to 7.9), but relatively low intercepts (5.8 to 8.7) values, reflecting the arid conditions of the northern Pacific domain (Loreto and Culiacan; Fig. 2).

Figure 6: Local meteoric water lines across Mexico between 2018-2021. Regions are color-coded.

5.5. Regional moisture sources

Figure 7A shows the location of six study regions (pink boxes) and their major annual climatological sources of moisture (E-P>0; in mm d^{-1}). To identify the sources, the air masses residing over each of the study regions were tracked backward in time from 1980-2018. Areas shaded by reddish colors in the (E-P) pattern represent regions where evaporation exceeded precipitation in the net moisture budget (E-P >

0) and denote the most relevant moisture sources throughout the hydrological year. According to this, parts of the Gulf of Mexico, the Caribbean Sea, the Pacific Ocean, and also terrestrial regions are identified as the main sources of moisture contributors to the precipitation over the Mexican target regions. Afterward, a forward-in-time analysis of air masses residing over the sources was performed to compute their contribution to the precipitation over each study region. This contribution is assumed as the negative values on a budget of the evaporation minus precipitation (E-P<0; where precipitation exceeds evaporation). Figure 7B represents the long-term annual climatological precipitation cycle (mm/month) (1980-2018) for each of the six sink regions across Mexico and the overall moisture source contribution from each domain. In the Northern Plateau, the NAMS is clearly depicted by greater precipitation amounts between June and September, with the largest terrestrial moisture input (20.5%) [61, 87]. In the North Pacific region, the combination of tropical storms, monsoonal rainfall, and terrestrial sources governed precipitation inputs mainly between May and November [8, 88]. The Northern Gulf region exhibited nearly uniform moisture contributions from the Pacific Ocean and terrestrial sources throughout the year, and a major input from the Gulf of Mexico basin (38.7%) from May to October [61, 89]. In the Central Plateau, where the City of Mexico is located, the bimodal precipitation cycle is constrained by a major moisture contribution from the Gulf of Mexico (44.2%), and similar inputs from the Pacific Ocean (27.0%) and the Caribbean basin (27.1%). In the wettest southern lowland region, moisture sources from the Pacific Ocean (33.4%) and the Gulf of Mexico (39.1%) play a predominant role in rainfall generation, with less influence

from the Caribbean basin (16.4%) [69]. A similar pattern is observed for the South Pacific domain with minimal terrestrial inputs and large oceanic contributions.

Figure 7: Atmospheric moisture source-sink analysis: A) Spatial distribution of annual moisture source (E-P>0) (in mm d^{-1}) for the study regions (pink polygons). Red areas denote moisture sources. B) Climatological annual cycle of precipitation (mm/month) per region: i) Central Plateau, ii) North Pacific coast, iii) Northern Gulf coast, iv) Northern Plateau, v) South Pacific coast, and vi) Southern Gulf coast. Moisture sources are color-coded: Caribbean basin (yellow), Gulf of Mexico (green), Pacific Ocean (cyan), and terrestrial (blue). The pie charts show the moisture source contribution to the annual precipitation cycle. Period of study: 1980-2018.

5.6. Isoscape models

Isoscape models based on topographic and geographic regressors accurately captured the isotopic variability across the complex physiographic units of Mexico (Fig. 8). Depleted values are distributed across both main cordilleras and southernmost ranges, while enriched values are commonly found across the coastal domains and northern regions. The $\delta^{18}O$ isoscape ranged from -13.39 to -2.75‰ (Fig. 8A), whereas $\delta^{2}H$ varied from -96.83 to -9.89‰ (Fig. 8D). Residual analysis denoted a strong agreement with the observed isotope ratios (*Adj.* r^2=0.84 for $\delta^{18}O$ and *Adj.* r^2=0.86 for $\delta^{2}H$; Figs. 8C and 8F). Previous global isoscape products [54] based on absolute latitude and elevation (i.e., temperature-driven effects) regressors (Figs. 8B and 8E) exhibited a slightly lower agreement with the observed isotope ratios (*Adj.* r^2=0.77 for $\delta^{18}O$ and *Adj.* r^2=0.77 for $\delta^{2}H$; Figs. 8C and 8F). The latter might be explained by the coarser resolution of the global grid [54] compared to the updated isoscapes presented in this study (100 m^2 grid). However, this global product reported more enriched compositions across the Pacific coast and the Gulf of California than the observed values. The spatial *d*-excess variability was computed based on $\delta^{18}O$ and $\delta^{2}H$ raster outputs (Fig. 9). In this study, *d*-excess varied from 8.35‰ (northern regions) to 13.22‰ (southern regions), whereas the global product varied from -4.78‰ (northern regions) to 17.87‰ (central and northern plateaus). Overall, both models performed poorly compared to the precipitation-weighted *d*-excess values (Fig. 9C), highlighting the need to constrain terrestrial moisture inputs in the evolution of precipitation systems across Mexico [95].

Figure 8: Mean annual isoscape models for $\delta^{18}O$ and $\delta^{2}H$ (this study; A and D) versus a global product (B and E) from [54]. Panels C and F show the goodness-of-fit between observed (precipitation-weighted) and predicted $\delta^{18}O/\delta^{2}H$ values. Isoscape models based on topographic (elevation) and geographical predictors (latitude and longitude) (orange squares) resulted in an overall improvement ($\delta^{18}O$; *Adj.* r^2=0.84 and $\delta^{2}H$; *Adj.* r^2=0.86) when compared to global products (gray-dots) based on absolute latitude and elevation (i.e., temperature-driven effects) regressors.

Figure 9: Mean annual isoscape model for *d*-excess (this study; A) versus a global product (B) from [54]. Panel C shows the goodness-of-fit between observed (precipitation-weighted) and predicted *d*-excess values. Both models exhibited poor performance when compared to precipitation-weighted *d*-excess values across Mexico.

6. Discussion

6.1. Spatial isotopic variations in precipitation across Mexico

Isotope variations in meteoric water are a product of the interactions between topography (e.g., mountain ranges, depressions, inter-mountainous valleys), vapor transport (e.g., Pacific Ocean, Gulf of Mexico, Caribbean Sea, and terrestrial sources), and the influence of recycled moisture (i.e., evapotranspiration) (Fig. 2) [90-92]. These features interplay in a complex array of physiographic units across Mexico, resulting in challenging spatial isotope patterns (Figs. 8 and 9).

Tropical cyclones contribute up to 40% to the annual rainfall in the coastal regions of northwestern Mexico (e.g., Loreto and Hermosillo; Fig. 1) [97], whereas annual contributions range between 20-30% along the Gulf of Mexico coast. During active hurricane seasons, these storms can result in abundant and enriched rainfall in the Gulf of Mexico and Caribbean Sea coast, and in depleted compositions inland (i.e., orographic distillation) and along the northwestern Pacific coast [8, 98]. Cold fronts and atmospheric rivers are also responsible for depleted isotopic compositions in across the northwestern region, with $\delta^{18}O$ up to -15‰ during the boreal winter in the northern plateau (Fig. 3B). The NAMS activation commonly results in large precipitation events, highly localized, and enriched across the northwestern and north central regions of Mexico [22, 81, 82]. The latter is clearly depicted by the inverse (positive) precipitation amount relationships (Fig. 4). In contrast, the northerly trade winds and easterly waves result in enriched compositions along the Gulf of Mexico and Yucatan peninsula [10, 12]. The convergence of the northerly trade winds with the southerly trade winds across orographic barriers results in depleted compositions during the summer over central Mexico (Fig. 3B).

The stronger rainout effect (i.e., a progressive isotope depletion in precipitation with increasing distance from the ocean) observed over the GCS domain is most likely related to the direct influence of the trade winds and nearby moisture transport from the Gulf of Mexico and the Caribbean Sea basins (Fig. 6A). In the intramountainous plateaus and the Pacific slope, the combination of the rain shadow effect (i.e., an area of significantly reduced precipitation behind a mountainous region), more complex and rugged topography, recycled evapotranspiration, deep convective activity (June-September), and indirect influence of tropical cyclones results in weaker and more complex spatial trends [72]. In this regard, the isotopic bias introduced in low-elevation coastal stations affected by tropical storms within the Mesoamerican region should be considered when determining isotopic lapse rates for hydrogeological applications (e.g., mean recharge elevations). For instance, low-elevation sites (i.e., Loreto, Culiacan, and Hermosillo; Fig. 1) across the northern Pacific coast were affected by strong hurricane landfalls and passages during the monitoring period (e.g., hurricanes Rosa-2018 and Sergio-2018, Lorena-2019, Nora-2021, and Pamela-2021, among other tropical storms). Remarkably, [8] reported a relatively weak isotope lapse rate within the Sonora River basin (PC to NP) during the wet season (-1.1‰ in $\delta^{18}O$ per km of elevation) but noted that the isotope lapse rate increased (intra-seasonally) due to tropical cyclone events (-2.6‰ in $\delta^{18}O$ per km of elevation; *Adj.* r^2 = 0.86; $p<0.001$).

In Mexico, the nationwide isotopic lapse rate (based on arithmetic means) can be defined as -1.75‰ in $\delta^{18}O$ per km of elevation (*Adj.* r^2=0.65, $p<0.001$; Fig. 5), whereas the precipitation-weighted lapse rate can be described as -2.10‰ in $\delta^{18}O$ per km of elevation (72% of the total variance explained, $p<0.001$; Fig. 5). The lapse rate obtained in the isoscape modeling resulted in -1.72 $\delta^{18}O$/km.

Overall, the reported isotope lapse rates agree with previous studies (-2.3‰/km) based on a combined approach of regressing the mean $\delta^{18}O$ from GNIP stations against geographical and climatic regressors and applying the resulting function onto gridded climate data [51]. For instance, [72] reported a pantropical spectrum of isotopic lapse rates ranging from -3.5 to -0.5‰/km, with a pantropical mean of -2.2‰/km. Similarly, [92] reported a global isotopic lapse rate of -2.8‰/km. A previous groundwater isoscape effort in Mexico [22] evaluated 19 linear regression models, from a single variable model (elevation) to more complex iterations including drainage or slope (Pacific versus Gulf of Mexico and the Caribbean Sea basins), distance to coast, latitude, annual precipitation, and interaction among these variables. In the best model, elevation explained only 44% of the total variance in groundwater samples, while precipitation amount (10%), slope (Pacific versus GCS) (12%), and latitude (10%) explained a third of the total variance. Landscape damping effects in transitional regions from tropical to arid sub-tropical biomes can explain the relatively weaker elevation relationship in groundwater (e.g., secondary soil evaporation). In Costa Rica and Guatemala/Belize, [55, 96] reported similar lapse rates in precipitation, groundwater, and surface water (-2.5% in $\delta^{18}O$ per km) across the wet Caribbean slope, whereas weaker relationships have been reported across the dry Corridor of Central America (-1.0% in $\delta^{18}O$ per km) [51].

The updated spatial and temporal coverage of the Mexican isotope network (i.e., RENIP) facilitated a more robust representation of the meteoric isotope variability. In our model, 85% ($\delta^{18}O$) and 88% ($\delta^{2}H$) of the total variance is explained by topographic (elevation) and geographical regressors (latitude and longitude) , with $\delta^{18}O$ and $\delta^{2}H$ residuals varying from +2.0‰ (Ciudad Victoria; northern region) to -1.2‰ (Tulancingo; central region). On average, the predicted mean annual $\delta^{18}O$ compositions were more depleted across the central (0.04‰) and northern (0.27‰) plateaus, except for Hermosillo (coastal site affected by tropical storms) (more enriched by 0.58‰) and Pachuca (high elevation site; 2,365 m asl) (more enriched by 1.06‰) sites. The larger residual variability was observed across the Gulf of Mexico and Caribbean Sea sites with residuals ranging from 2.0‰ (Ciudad Victoria; northern coast) to -0.90‰ (Mérida; southern coast). In contrast, the predicted mean annual $\delta^{18}O$ compositions across the Pacific coast sites were consistently under-predicted on average by -0.48‰, indicating the tropical cyclone bias affecting this region.

7. Conclusions

This synthesis of stable isotope compositions in precipitation across distinct landscapes of Mexico shows how complex atmospheric processes and moisture contributions from terrestrial and maritime (the Pacific Ocean, Gulf of Mexico, and the Caribbean Sea basin) domains interplay with topographic features, resulting in isotopic spatial and temporal variations throughout the hydrological year. In this regard, water vapor sampling or high-frequency discrete samples [93, 94] are still needed to clearly separate the role of terrestrial (e.g., local and remote transpiration, ground evaporation, and canopy evaporation) [95] versus oceanic moisture in controlling the observed spatial isotope variability, with particular interest across the north Pacific coast and northern plateau region.

The inherent complexity of observed monthly precipitation relationships across Mexico invokes the need to underpin the local (e.g., precipitable water column) and regional weather processes governing the spatial trends. The latter also precludes using the classical amount effect as a valid regressor. In the northern regions, terrestrial and maritime moisture sources resulted in enriched isotope compositions during the monsoon season. The latter is further evidenced by inverse (positive) precipitation amount and $\delta^{18}O$ relationship in Torreon, Hermosillo, Piedras

Negras, Durango, and Chihuahua (+0.4 to +2.3‰ in $\delta^{18}O$/100 mm). Windward (Gulf of Mexico coast) and high mountainous regions exhibited moderate to strong effects (-0.2 to -2.2‰ in $\delta^{18}O$/100 mm). Lowland arid regions across the north Pacific resulted in poor relationships (-0.8 to +0.01‰ in $\delta^{18}O$/100 mm) mostly affected by the indirect effect of tropical cyclones. In the central, southern Gulf coast, and south Pacific regions oceanic moisture sources were dominant (Gulf of Mexico>Pacific Ocean>Caribbean Sea). On the northeastern coast, moisture from the Gulf of Mexico predominated as the main contributor.

The first attempt at building a high-resolution (100 m^2 grid) nationwide rainfall isoscape highlighted areas with significant spatial variability such as the Pacific coast and the northern arid regions, which highlights the need for additional monitoring efforts (per region) focused on the temporal bias produced by the indirect or direct effect of tropical cyclones, monsoon activity, and evapotranspiration moisture inputs. Our results fill a recognized historical gap in the precipitation isotope monitoring in North America and will provide a baseline to pursue more detailed ecohydrological, climatic, forensic, archeological, and paleoclimate studies across Mexico.

Acknowledgments

The National Monitoring Network of Isotopes in Precipitation (known as RENIP) across Mexico is the result of technical cooperation with the International Atomic Energy Agency (IAEA), through the Regional Project RLA/7/024 ‘Integration of Isotope Hydrology in National Assessments of Water Resources’. RSM thanks the STARs Program (Project Number AR911486) and the Office of the Provost funds at the university of Texas-Arlington (Project Number 314075) for their support. The authors also recognized the crucial partnership between the National Meteorological

Service and the Mexico City Water System. The Xunta of Galicia supported M.S. under postdoctoral grant ED481B-2021/134. EphysLab, Uvigo, received support from the Xunta de Galicia under Project ED431C 2021/44 (Programa de Consolidación e Estructuración de Unidades de investigación Competitivas (Grupos de Referencia Competitiva) and Consellería de Cultura, Educación e Universidade). The authors thank the multiple helping hands that contribute to precipitation sampling across Mexico.

References

1. Cortes A, Farvolden RN. Isotope study of precipitation and groundwater in the Sierra de Las Cruces, Mexico. Journal of Hydrology. 1989; 107(1-4): 147–153. https://doi.org/10.1016/0022-1694(89)90055-3.
2. Cortés A, Durazo J, Farvolden RN. Studies of isotopic hydrology of the basin of Mexico and vicinity: Annotated bibliography and interpretation. Journal of Hydrology. 1997; 198(1-4): 346–376. https://doi.org/10.1016/s0022-1694(96)03273-8.
3. Ortega-Guerrero A, Cherry JA, Aravena, R. Origin of pore water and salinity in the Lacustrine Aquitard overlying the Regional Aquifer of Mexico City. Journal of Hydrology. 1997; 197(1-4), 47–69. https://doi.org/10.1016/s0022-1694(96)03280-5.
4. Peñuela-Arévalo LA, Carrillo-Rivera JJ. Discharge areas as a useful tool for understanding recharge areas, study case: Mexico Catchment. Environ Earth Sci. 2013; 68, 999–1013. https://doi.org/10.1007/s12665-012-1803-z
5. Aguilar-Ramírez CF, Camprubí A, Fitz-Díaz E, Cienfuegos-Alvarado E, and Morales-Puente P. Variation in isotopic composition of meteoric water along the central-northeastern section of the Mexican Fold-and-Thrust Belt, Sierra Madre Oriental. Boletín de la Sociedad Geológica Mexicana. 2017; 69(2): 447-463. https://doi.org/10.18268/bsgm2017v69n2a9
6. Rivera-Rivera DM, Chidambaram S, Tirumalesh K, Escobedo-Urias DC, Sujitha SB, Rodriguez-Espinosa PF, Devaraj N, Sinha UK, Jonathan MP. Stable isotopic (δ2H, δ18O) monograms of winter precipitation events and hydro-climatic dynamics in Central Mexico. Atmospheric Research. 2021; 261: 105744. https://doi.org/10.1016/j.atmosres.2021.105744
7. Johannesson KH, Cortés A, Kilroy KC. Reconnaissance isotopic and hydrochemical study of Cuatro Ciénegas groundwater, Coahuila, Mexico. Journal of South American Earth Sciences. 2004; 17(2): 171-180. https://doi.org/10.1016/j.jsames.2004.01.002

8. Pérez-Quezadas JP, Adams D, Sánchez-Murillo R, Lagunes AJ, Castañeda JLR. Isotopic variability (δ18O, δ2H and d-excess) during rainfall events of the north American monsoon across the Sonora River Basin, Mexico. Journal of South American Earth Sciences. 2021; 105: 102928. https://doi.org/10.1016/j.jsames.2020.102928
9. González-Hita L, Mejía-González MA, Carteño-Martinez B, et al. 2021. Isotopic composition of rainfall in Baja California Sur, Mexico. Int J Hydro. 5(3):93-100. DOI: 10.15406/ijh.2021.05.00271
10. Pérez-Quezadas JP, Silva AC, Inguaggiato S, Ortega MDRS, Pérez JC, Heilweil VM. 2015. Meteoric isotopic gradient on the windward side of the Sierra Madre Oriental area, Veracruz–Mexico. Geofísica internacional, 54(3), 267-276. https://doi.org/10.1016/j.gi.2015.04.021
11. Lases-Hernandez F, Medina-Elizalde M, Burns S, DeCesare M. Long-term monitoring of drip water and groundwater stable isotopic variability in the Yucatán Peninsula: Implications for recharge and speleothem rainfall reconstruction. Geochimica et Cosmochimica Acta. 2019; 246: 41-59. https://doi.org/10.1016/j.gca.2018.11.028
12. Cejudo E, Acosta-González G, Leal-Bautista RM. Regional meteoric water line of the Yucatan Peninsula, Mexico. Geosci Data J. 2021; 1–7. https://doi.org/10.1002/gdj3.123
13. GNIP (Global Network of Isotopes in Precipitation). 2022. Available from: http://wwwnaweb.iaea.org/napc/ih/I_resources_gnip.html.
14. Moreiras-Reynaga DK, Millaire JF, Balderas XC, Berrelleza JAR, Luján LL, Longstaffe FJ. Building Mexican isoscapes: Oxygen and hydrogen isotope data of meteoric water sampled across Mexico. Data Brief. 2021: 36:107084. Doi: 10.1016/j.dib.2021.107084.
15. García E. Distribución de la precipitación en la República Mexicana. Investigaciones Geográficas. 2003; 50: 67-76. http://www.scielo.org.mx/pdf/igeo/n50/n50a9.pdf
16. Garreaud R. Subtropical cold surges: Regional aspects and global distribution. International Journal of Climatology. 2001; 21:1181-1197. https://doi.org/10.1002/joc.687
17. Martínez-Claros J, Raymond DJ, Fuchs-Stone Ž. Vorticity and Thermodynamics in a Gulf of Mexico Atmospheric River. Atmósfera. 2022; 35(2), 273–286. https://doi.org/10.20937/ATM.52901.
18. Dominguez C, Done JM, Bruyère CL. Easterly wave contributions to seasonal rainfall over the tropical Americas in observations and a regional climate model. Climate Dynamics. 2020; 54: 191–209. https://doi.org/10.1007/s00382-019-04996-7.
19. Breña-Naranjo JA, Pedrozo-Acuña A, Pozos-Estrada O, Jiménez-López SA, López-López MR. The contribution of tropical cyclones to rainfall in Mexico. Physics and Chemistry of the Earth. 2015; 83-84: 111-122. https://doi.org/10.1016/j.pce.2015.05.011
20. Peel MC, Finlayson BL, McMahon TA. Updated world map of the Köppen-Geiger climate classification. Hydrology and earth system sciences. 2007; 11(5): 1633-1644. https://doi.org/10.5194/hess-11-1633-2007

21. Bowen GJ. Isoscapes: spatial pattern in isotopic biogeochemistry. Annual review of earth and planetary sciences. 2010; 38: 161-187. https://doi.org/10.1146/annurev-earth-040809-152429
22. Wassenaar LI, Van Wilgenburg SL, Larson K, Hobson KA. A groundwater isoscape (δD, δ18O) for Mexico. Journal of Geochemical Exploration. 2009; 102(3): 123–136. Doi:10.1016/j.gexplo.2009.01.0.
23. Hobson KA, Van Wilgenburg SL, Larson K, Wassenaar LI. A feather hydrogen isoscape for Mexico. Journal of Geochemical Exploration. 2009;102(3):167-74. https://doi.org/10.1016/j.gexplo.2009.02.007
24. Ammer ST, Bartelink EJ, Vollner JM, Anderson BE, Cunha EM. Spatial distributions of oxygen stable isotope ratios in tap water from Mexico for region of origin predictions of unidentified border crossers. Journal of Forensic Sciences. 2020 65(4): 1049-1055. https://doi.org/10.1111/1556-4029.14283
25. Fan M, Foote JM, Martin AJ, Zhu L. Stable isotope compositions of surface water in Mexico between 22–26° N. Journal of South American Earth Sciences. 2022. 103723. https://doi.org/10.1016/j.jsames.2022.103723
26. Escobar M, Hoyos I, Nieto R, Villegas JC. The importance of continental evaporation for precipitation in Colombia: A baseline combining observations from stable isotopes and modelling moisture trajectories. Hydrological Processes. 2022; 36(6): e14595. https://doi.org/10.1002/hyp.14595
27. Álvarez M. Provincias fisiográficas de la República Mexicana. Boletín de la Sociedad Geológica Mexicana. 1961; 24(2): 5-20. https://www.jstor.org/stable/44173915
28. García-Arizaga MT, Lugo HJ. El relieve mexicano en mapas topográficos. Serie Libros No. 5. 2003:148. Instituto de Geografía, UNAM, Mexico. Available from: http://www.publicaciones.igg.unam.mx/index.php/ig/catalog/book/81
29. Schultz D, Bracken WE, Bosart LF. Planetary- and synoptic-scale signatures associated with Central American cold surges. Monthly Weather Review. 1998; 126: 5–27. DOI:10.1175/1520-0493(1998)126<0005:PASSSA>2.0.CO;2
30. Henry WK. Some aspects of the fate of cold fronts in the Gulf of Mexico. Monthly Weather Review. 1979; 107: 1078-1082. https://doi.org/10.1175/1520-0493(1979)107<1078:SAOTFO>2.0.CO;2
31. Reding PJ. The Central American cold surges: An observational analysis of the deep southward penetration of North America cold fronts. M.Sc. Thesis. Department of Meteorology, Texas A&M University. 1992; Available from: https://apps.dtic.mil/sti/pdfs/ADA268592.pdf
32. Schultz DM, Bracken WE, Bosart LF, Hakim GJ, Bedrick MA, Dickinson MJ, Tyle KR. The 1993 Superstorm cold surge: frontal structure, gap flow and tropical impact. Monthly Weather Review. 1997; 125: 5-39. https://doi.org/10.1175/1520-0493(1997)125<0005:TSCSFS>2.0.CO;2
33. Ralph FM, Dettinger MD. Storms, floods, and the science of atmospheric rivers. Eos Trans. Am. Geophys. Union. 2011; 92, 265–266. https://doi.org/10.1029/2011EO320001
34. Dettinger MD, Ralph FM, Das T, Neiman PJ, Cayan DR. Atmospheric Rivers, Floods and the Water Resources of California. Water. 2011; 3: 445-478; doi:10.3390/w3020445.

35. Vidal Zepeda R. Precipitación total anual. Hoja NA IV.5, esc. 1:8 000 000, Nuevo Atlas Nacional de Mexico, Instituto de Geografía, UNAM, Mexico. 2007.
36. Bao JW, Michelson SA, Neiman PJ, Ralph FM, Wilczak JM. Interpretation of enhanced integrated water vapor bands associated with extra-tropical cyclones: their formation and connection to tropical moisture. Mon. Wea. Rev. 2006; 134: 1063–1080. Doi: 10.1175/MWR3123.1
37. Gimeno L, Nieto R, Vázquez M, Lavers DA. Atmospheric Rivers: a mini-review. Frontiers in Earth Science. 2014; 2:2. https://doi.org/10.3389/feart.2014.00002
38. Douglas MW, Maddox RA, Howard K, Reyes S. The Mexican Monsoon. Journal of Climate. 1993; 6(8): 1665–1677. https://journals.ametsoc.org/view/journals/clim/6/8/1520-0442_1993_006_1665_tmm_2_0_co_2.xml
39. Pascale S, Kapnick SB, Bordoni S, Delworth TL. The Influence of CO2 Forcing on North American Monsoon Moisture Surges. Journal of Climate. 2018; 31(19): 7949–7968. Doi:10.1175/jcli-d-18-0007.1
40. Wang C, Lee S. Atlantic warm pool, Caribbean low-level jet, and their potential impact on Atlantic hurricanes. Geophysical Research Letters. 2007; 34: L02703, doi:10.1029/2006GL028579.
41. Davis RE, Hayden BP, Gay DA, Phillips WL, Jones GV. The North Atlantic Subtropical Anticyclone. Journal of Climate. 1997; 10:728-744. https://doi.org/10.1175/1520-0442(1997)010<0728:TNASA>2.0.CO;2
42. Romero-Centeno R, Zavala-Hidalgo J, Raga GB. Midsummer gap winds and low-level circulation over the eastern tropical Pacific. Journal of Climate. 2007; 20(15):3768-3784. https://doi.org/10.1175/JCLI4220.1
43. Jáuregui OE. Algunos conceptos modernos sobre la circulación general de la atmosfera. Investigaciones geográficas, Boletin del Instituto de Geografía. 2003; 50: 121-143.http://www.scielo.org.mx/scielo.php?script=sci_arttext&pid=S0188-46112003000100012
44. Dominguez C, Done JM, Bruyère CL. Easterly wave contributions to seasonal rainfall over the tropical Americas in observations and a regional climate model. Climate Dynamics. 2020;54(1):191-209.
45. Farfán LM, Alfaro EJ, Cavazos T. Characteristics of tropical cyclones making landfall on the Pacific coast of Mexico: 1970-2010. Atmósfera. 2013; 26(2): 163-182. https://doi.org/10.1016/S0187-6236(13)71070-1
46. Gröning M, Lutz HO, Roller-Lutz Z, Kralik M, Gourcy L, Pöltenstein L. A simple rain collector preventing water re-evaporation dedicated for $\delta^{18}O$ and $\delta^{2}H$ analysis of cumulative precipitation samples. Journal of Hydrology. 2012; 448–449: 195-200. https://doi.org/10.1016/j.jhydrol.2012.04.041
47. Funk C, Peterson P, Landsfeld M. et al. The climate hazards infrared precipitation with stations—a new environmental record for monitoring extremes. Sci Data 2. (2015); 150066. https://doi.org/10.1038/sdata.2015.66
48. González-Hita, L., R. Sánchez-Murillo, M. Mejía-González (2023). Isotope compositions in precipitation across Mexico: 2018-2021, HydroShare, http://www.hydroshare.org/resource/909aaa5edf1040b6a6244a0ca7f58890
49. Dansgaard W. Stable isotopes in precipitation. Tellus. 1964; 16(4):436–468.

50. Jasechko S, Taylor RG. Intensive rainfall recharges tropical groundwaters. Environmental Research Letters. 2015; 10(12): 124015. Doi:10.1088/1748-9326/10/12/124015
51. Sánchez-Murillo R, Esquivel-Hernández G, Corrales-Salazar, JL, Castro-Chacón L, Durán-Quesada AM, Guerrero-Hernández M, et al. Tracer hydrology of the data-scarce and heterogeneous Central American Isthmus. Hydrological Processes. 2020a; 34: 2660-2675. https://doi.org/10.1002/hyp.13758
52. Terzer S, Wassenaar L, Araguás-Araguás L, Aggarwal P. Global isoscapes for $\delta^{18}O$ and $\delta^{2}H$ in precipitation: Improved prediction using regionalized climatic regression models. Hydrology and Earth System Sciences. 2013; 17, 4713-4728. https://doi.org/10.5194/hess-17-4713-2013,2013
53. R Core Team. R: A language and environment for statistical computing. R Foundation for Statistical Computing, Vienna, Austria. 2022; Available from: https://www.R-project.org/
54. Bowen GJ, Revenaugh J. Interpolating the isotopic composition of modern meteoric precipitation, Water Resour. Res. (2003); 39, 1299, doi:10.1029/2003WR002086, 10.
55. Sánchez-Murillo R, Birkel C. Groundwater recharge mechanisms inferred from isoscapes in a complex tropical mountainous region. Geophysical Research Letters. 2016; 43(10):5060-9. https://doi.org/10.1002/2016GL068888
56. Budyko MI. On climatic factors of runoff. (in Russian). Probl. Fiz. Geogr. 1951; 16: 41–48.
57. Conagua. Compendio Básico del Agua en Mexico, Mexico. 2002. Available from https://www.gob.mx/cms/uploads/attachment/file/259365/_2001_CBA2001.pdf
58. Fu B. 1981. On the calculation of the evaporation from land surface [in Chinese]. Chinese Journal of Atmospheric Sciences. 1981; 5(1): 23-31. Doi: 10.3878/j.issn.1006-9895.1981.01.03
59. Zhang L*,* Hickel *K,* Dawes WR*,* Chiew FHS*,* Western AW*,* Briggs PR*.* A rational function approach for estimating mean annual evapotranspiration*,* Water Resour. Res. *2004;* 40*, W02502, doi:*10.1029/2003WR002710*.*
60. Anderson BT. Roads JO. Summertime moisture divergence over the southwestern US and northwestern Mexico. Geophysical Research Letters. 2001; 28(10): 1973-1976. https://doi.org/10.1029/2001GL012903
61. Hu H, Dominguez F. Evaluation of oceanic and terrestrial sources of moisture for the North American monsoon using numerical models and precipitation stable isotopes. Journal of Hydrometeorology. 2015; 16(1): 19-35. https://doi.org/10.1175/JHM-D-14-0073.1
62. Ordoñez P, Nieto R, Gimeno L, Ribera P, Gallego D, Ochoa-Moya CA, Quintanar AI. Climatological moisture sources for the Western North American Monsoon through a Lagrangian approach: their influence on precipitation intensity. Earth System Dynamics. 2019; 10(1): 59-72. https://doi.org/10.5194/esd-10-59-2019
63. Perdigón-Morales J, Romero-Centeno R, Ordoñez P, Nieto R, Gimeno L, Barrett BS. Influence of the Madden-Julian oscillation on moisture transport by the Caribbean low level jet during the midsummer drought in Mexico. Atmospheric Research. 2021; 248 :105243. https://doi.org/10.1016/j.atmosres.2020.105243
64. Stohl A, James P. A Lagrangian analysis of the atmospheric branch of the global water cycle. Part I: method description, validation, and demonstration for the

August 2002 flooding in central Europe. J. Hydrometeorol. 2004; 5: 656–678. https://doi.org/10.1175/1525-7541(2004)005<0656:ALAOTA>2.0.CO;2
65. Pisso I, Sollum E, et al. The Lagrangian particle dispersion model FLEXPART version 10.4, Geosci. Model Dev. 2019; 12, 4955–4997, https://doi.org/10.5194/gmd-12-4955-2019.
66. Frank A, Seibert P, Wotawa G. Technical note: the Lagrangian particle dispersion model FLEXPART version 6.2. Atmos. Chem. Phys. 2005; 5: 2461–2474. https://doi.org/10.5194/acp-5-2461-2005, 2005.
67. Nieto R, Gimeno L. A database of optimal integration times for Lagrangian studies of atmospheric moisture sources and sinks. Sci Data. 2019; 6: 59. https://doi.org/10.1038/s41597-019-0068-8
68. Stohl A, Forster C, Frank A, Seibert P, Wotawa G. The Lagrangian particle dispersion model FLEXPART version 6.2. Atmospheric Chemistry and Physics. 2005;5(9):2461-74.
69. Gimeno L, Drumond A, Nieto R, Trigo RM, Stohl A. On the origin of continental precipitation, Geophys. Res. Lett. 2010; 37: L13804, https://doi.org/10.1029/2010GL043712
70. Gimeno L, Nieto R, Sorí R. The growing importance of oceanic moisture sources for continental precipitation. Npj. Clim. Atmos. Sci. 2020; 3: 27. https://doi.org/10.1038/s41612-020-00133-y
71. Putman AL, Fiorella RP, Bowen GJ, Cai Z. A Global Perspective on Local Meteoric Water Lines: Meta-analytic Insight into Fundamental Controls and Practical Constraints. Water Resources Research. 2019; 55 (8). Doi:10.1029/2019wr02518.
72. Sánchez-Murillo R, Esquivel-Hernández G, Birkel C, Correa A, Welsh K, Durán-Quesada AM, Sánchez-Gutiérrez R, Poca M. Tracing Water Sources and Fluxes in a Dynamic Tropical Environment: From Observations to Modeling. Front. Earth Sci. 2020b; 8:571477. Doi: 10.3389/feart.2020.571477.
73. Jasechko S, Sharp Z, Gibson J, Jean Birks S, Yi Y, Fawcett, PJ. Terrestrial water fluxes dominated by transpiration. Nature. 2013; 496: 347–350. Doi:10.1038/nature11983
74. Wei Z, Yoshimura K, Wang L, Miralles DG, Jasechko S, Lee X. Revisiting the contribution of transpiration to global terrestrial evapotranspiration. Geophys. Res. Lett. 2017; 44, 2792–2801, doi:10.1002/2016GL072235.
75. Hoerling M, Barsugli J, Livneh B, Eischeid J, Quan X, Badger A. Causes for the Century-Long Decline in Colorado River Flow, Journal of Climate. 2019; 32(23): 8181-8203. https://journals.ametsoc.org/view/journals/clim/32/23/jcli-d-19-0207.1.xml
76. Esquivel-Hernández G, Sánchez-Murillo R, Birkel C, Good SP, Boll J. Hydroclimatic and ecohydrological resistance/resilience conditions across tropical biomes of Costa Rica. Ecohydrology. 2017; 10:e1860. https://doi.org/10.1002/eco.1860
77. Jones J, Creed I, Hatcher KL, Warren RJ, Adams MB, Benson MH, et al. Ecosystem Processes and Human Influences Regulate Streamflow Response to Climate Change at Long-Term Ecological Research Sites, BioScience. 2012; 62(4): 390–404, https://doi.org/10.1525/bio.2012.62.4.10

78. Magaña VO, Vázquez JL, Pérez JL, Pérez JB. Impact of El Niño on precipitation in Mexico. Geofísica internacional. 2003; 42(3): 313-330. https://www.redalyc.org/articulo.oa?id=56842304
79. Adams DK, Comrie, AC. The North American Monsoon. Bulletin of the American Meteorological Society. 1997; 78(10): 2197-2214. https://journals.ametsoc.org/view/journals/bams/78/10/1520-0477_1997_078_2197_tnam_2_0_co_2.xml
80. Becker E. The North America Monsoon. NOAA. 2022. Available from: https://www.climate.gov/news-features/blogs/enso/north-american-monsoon
81. Eastoe CJ, Dettman DL. Isotope amount effects in hydrologic and climate reconstructions of monsoon climates: implications of some long-term data sets for precipitation. Chem. Geol. 2016; 430, 78–89. https://doi.org/10.1016/j.chemgeo.2016.03.022
82. Eastoe CJ, Wright WE. Hydrology of mountain blocks in Arizona and New Mexico as revealed by isotopes in groundwater and precipitation. Geosciences. 2019: 119:461. Doi:10.3390/geosciences9110461
83. Scholl MA, Shanley JB, Zegarra JP, Coplen TB. The stable isotope amount effect: New insights from NEXRAD echo tops, Luquillo Mountains, Puerto Rico, Water Resour. Res. 2009; 45, W12407, doi:10.1029/2008WR007515.
84. Scholl MA, Murphy SF. Precipitation isotopes link regional climate patterns to water supply in a tropical mountain forest, eastern Puerto Rico, Water Resour. Res. 2014; 50, 4305– 4322, doi:10.1002/2013WR014413.
85. Sánchez-Murillo R, Birkel C, Welsh K, Esquivel-Hernández G, Corrales-Salazar J, Boll J, Brooks E, Roupsard O, Sáenz-Rosales O, Katchan I, Arce-Mesén R, Soulsby C, Araguás-Araguás LJ. Key drivers controlling stable isotope variations in daily precipitation of Costa Rica: Caribbean Sea versus Eastern Pacific Ocean moisture sources. Quaternary Science Reviews. 2016; 131, 250-261, https://doi.org/10.1016/j.quascirev.2015.08.028.
86. Munksgaard NC, Kurita N, Sánchez-Murillo R. et al. Data Descriptor: Daily observations of stable isotope ratios of rainfall in the tropics. Sci Rep. 2019;9, 14419. https://doi.org/10.1038/s41598-019-50973-9
87. Gochis DJ, Brito-Castillo L, Shuttleworth WJ. Hydroclimatology of the North American Monsoon region in northwest Mexico. Journal of Hydrology. 2006; 316(1-4): 53-70. https://doi.org/10.1016/j.jhydrol.2005.04.021
88. Englehart PJ, Douglas AV. The role of eastern North Pacific tropical storms in the rainfall climatology of western Mexico. International Journal of Climatology: A Journal of the Royal Meteorological Society. 2001; 21(11): 1357-1370. https://doi.org/10.1002/joc.637
89. Hales Jr, John E. Southwestern United States summer monsoon source Gulf of Mexico or Pacific Ocean? Journal of Applied Meteorology and Climatology. 1974; 13(3): 331-342. https://doi.org/10.1175/1520-0450(1974)013<0331:SUSSMS>2.0.CO;2
90. Gonfiantini R, Roche MA, Olivry JC, Fontes JC, Zuppi GM. The altitude effect on the isotopic composition of tropical rains. Chemical Geology. 2001; 181(1-4): 147-167. https://doi.org/10.1016/S0009-2541(01)00279-0
91. Blisniuk PM, Stern LA. Stable isotope paleoaltimetry: A critical review. American Journal of Science. 2005; 305(10): 1033-1074; DOI: https://doi.org/10.2475/ajs.305.10.1033

92. Poage MA, Chamberlain CP. Empirical relationships between elevation and the stable isotope composition of precipitation and surface waters: considerations for studies of paleoelevation change. American Journal of Science. 2001; 1;301(1):1-5.
93. Kühnhammer K, Dahlmann A, Iraheta A, Gerchow M, Birkel C, Marshall JD, Beyer M. Continuous in situ measurements of water stable isotopes in soils, tree trunk and root xylem: Field approval. Rapid Communications in Mass Spectrometry. 2022; 36(5): e9232. https://doi.org/10.1002/rcm.9232
94. Sánchez-Murillo R, Todini-Zicavo D, Poca M, Birkel C, Esquivel-Hernández G, Chavarría MM, Zuecco G, Penna D. Dry season plant water sourcing in contrasting tropical ecosystems of Costa Rica. Ecohydrology. 2023. e2541. https://doi.org/10.1002/eco.2541
95. Harrington TS, Nusbaumer J, Skinner CB. The contribution of local and remote transpiration, ground evaporation, and canopy evaporation to precipitation across North America. Journal of Geophysical Research: Atmospheres. 2023. 128, e2022JD037290. https://doi.org/10.1029/2022JD037290
96. Lachniet MS, Patterson W P. Oxygen isotope values of precipitation and surface waters in northern Central America (Belize and Guatemala) are dominated by temperature and amount effects. Earth and Planetary Science Letters. 2009; 284(3-4), 435-446. https://doi.org/10.1016/j.epsl.2009.05.010
97. Breña-Naranjo JA, Pedrozo-Acuña A, Pozos-Estrada O, Jiménez-López S A, López-López M R. The contribution of tropical cyclones to rainfall in Mexico. Physics and Chemistry of the Earth, Parts A/B/C. 2015; 83, 111-122. https://doi.org/10.1016/j.pce.2015.05.011
98. Sánchez-Murillo R, Durán-Quesada AM, Esquivel-Hernández G, Rojas-Cantillano D, Birkel C, Welsh K, Sánchez-Llull M, et al. Deciphering key processes controlling rainfall isotopic variability during extreme tropical cyclones. Nature communications. 2019; 10(1): 4321. https://doi.org/10.1038/s41467-019-12062-3

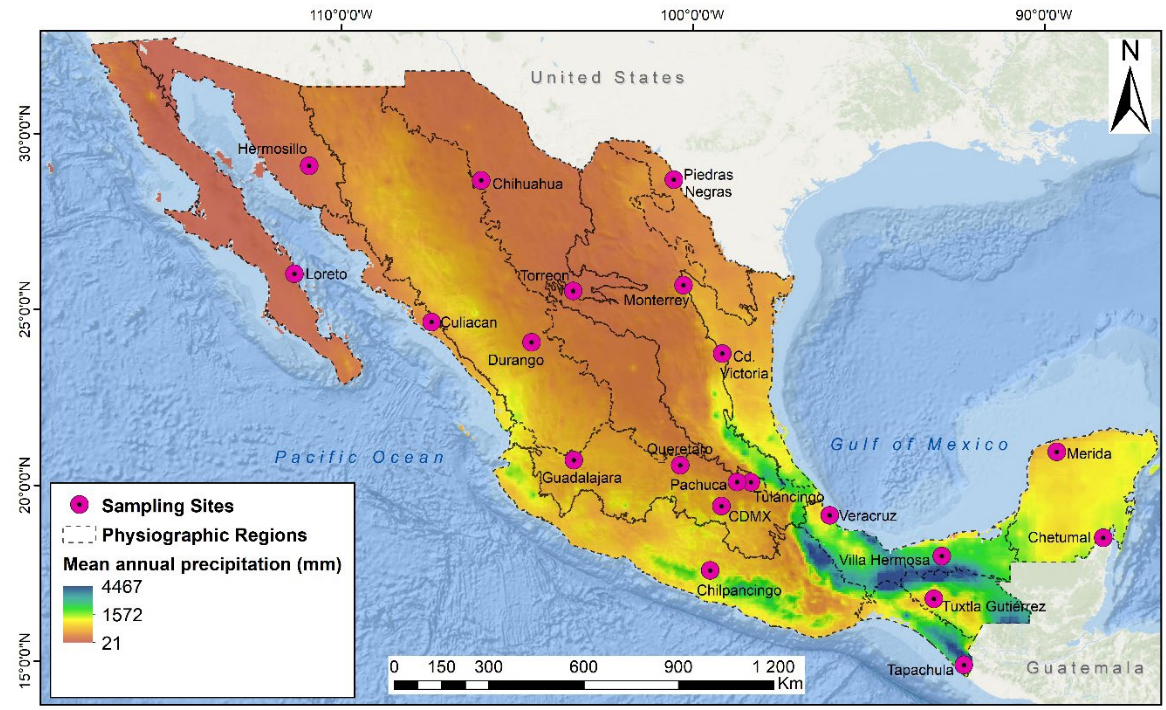

Figure 1: Map of Mexico including mean annual precipitation (mm) (1981-2019; based on CHIRPS data) [47], isotope monitoring sites (monthly sampling frequency; pink circles, dotted), and physiographic regions (dashed-line polygons; obtained from https://en.www.inegi.org.mx/temas/fisiografia/). The number of monitoring sites per physiographic region ranged from 1 to 5.

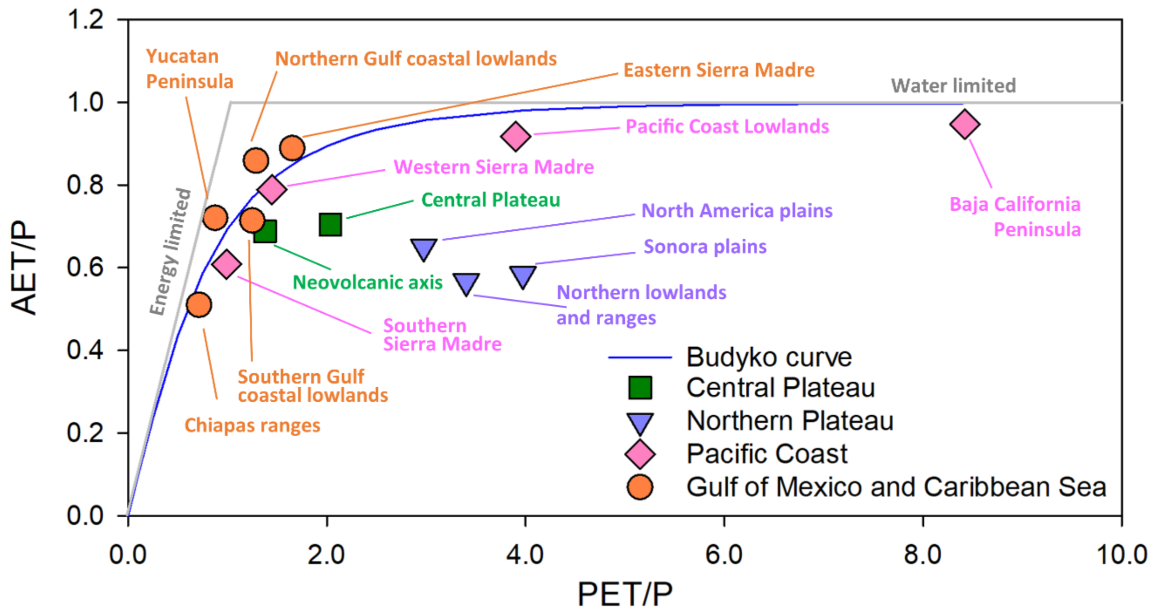

Figure 2: Budyko dual-space framework for the main physiographic regions (color coded). The X axis is the ratio of potential evapotranspiration (PET) to precipitation (P) (dryness index), and the Y axis represents the actual evapotranspiration (ET) over P (evaporative index). The blue line shows the 'Budyko curve' defined by ω=2.6 [54-55]. Grey solid lines define the energy and water limits.

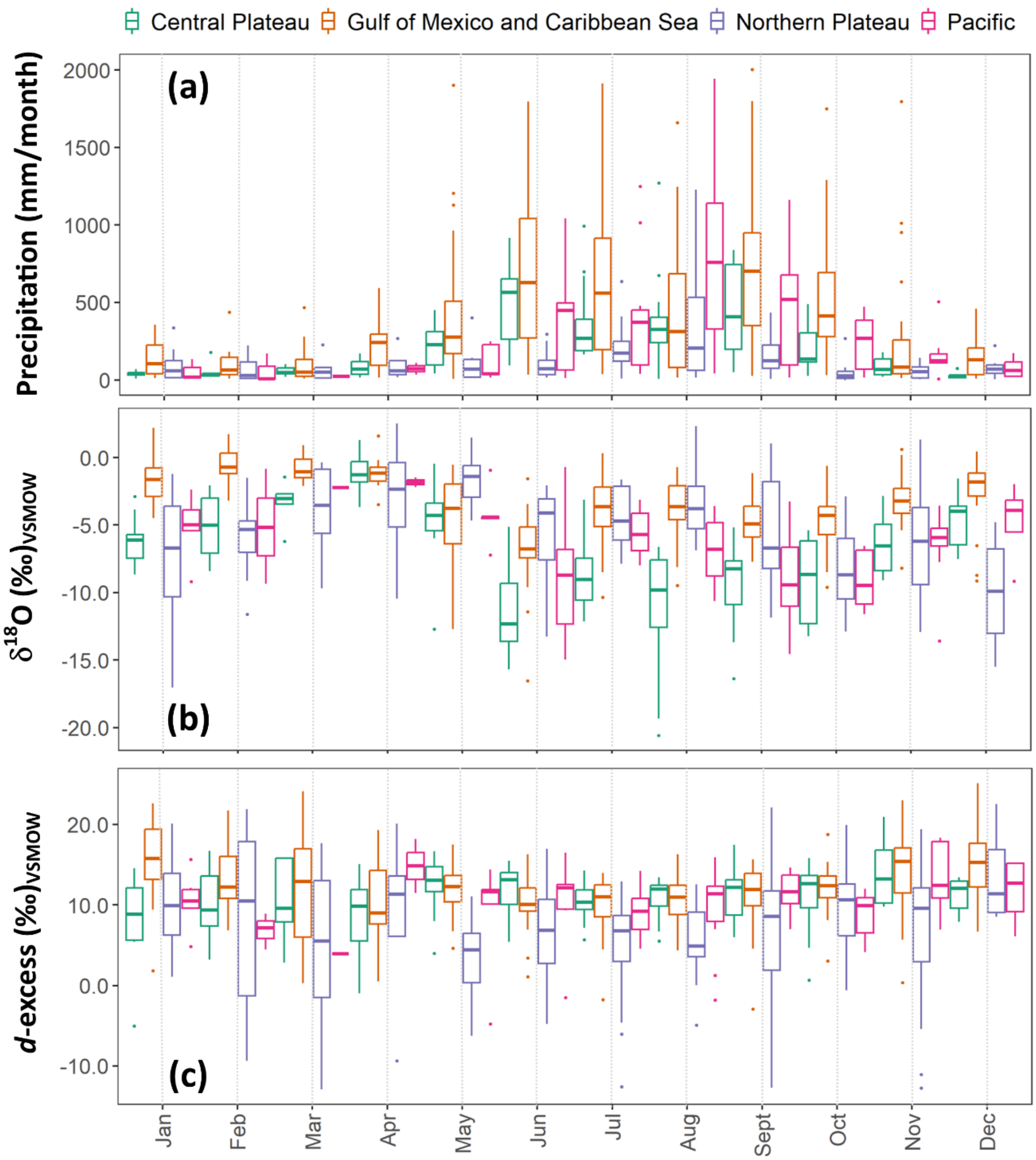

Figure 3: Monthly box plots of (a) precipitation (mm), (b) $\delta^{18}O$ (‰), and (c) *d*-excess (‰) for all monitoring sites in the Central Plateau (CP), the Gulf of Mexico and the Caribbean Sea coast (GCS), the Northern Plateau (NP), and the Pacific coast (PC).

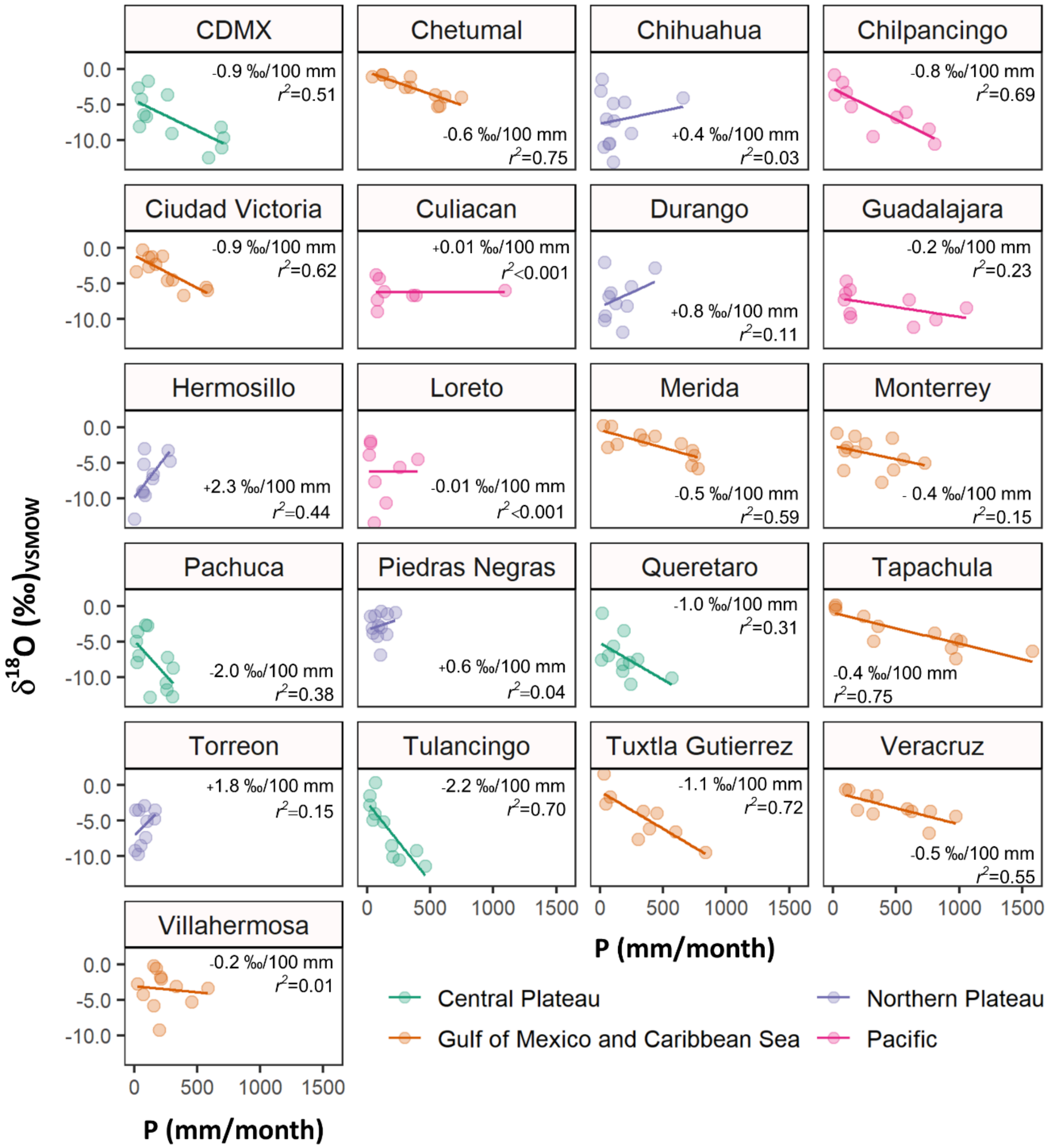

Figure 4: Monthly precipitation amount and $\delta^{18}O$ (‰) relationship per sampling site across Mexico. Regions are color-coded.

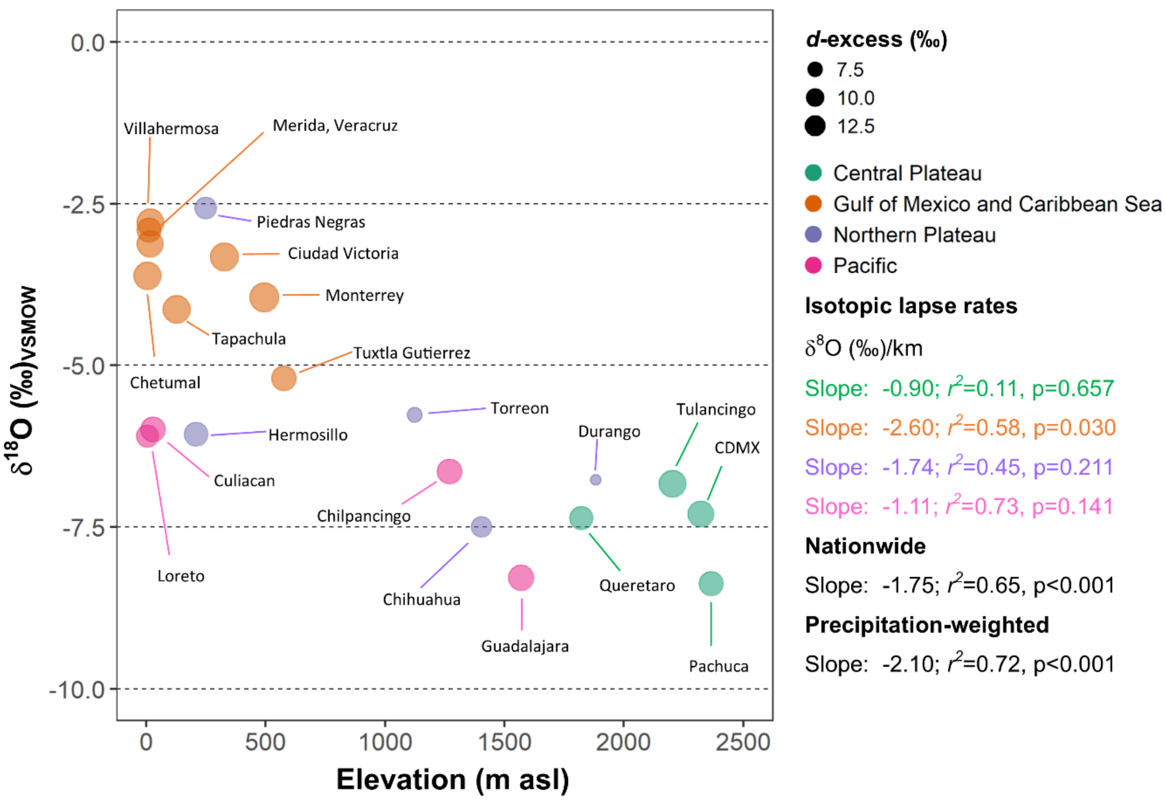

Figure 5: Elevation (m asl), $\delta^{18}O$ (‰), and *d*-excess (‰) relationship across Mexico. Regional isotopic lapse rates are color-coded and ranged from -0.90 to -2.60 ‰ in $\delta^{18}O$ per km.

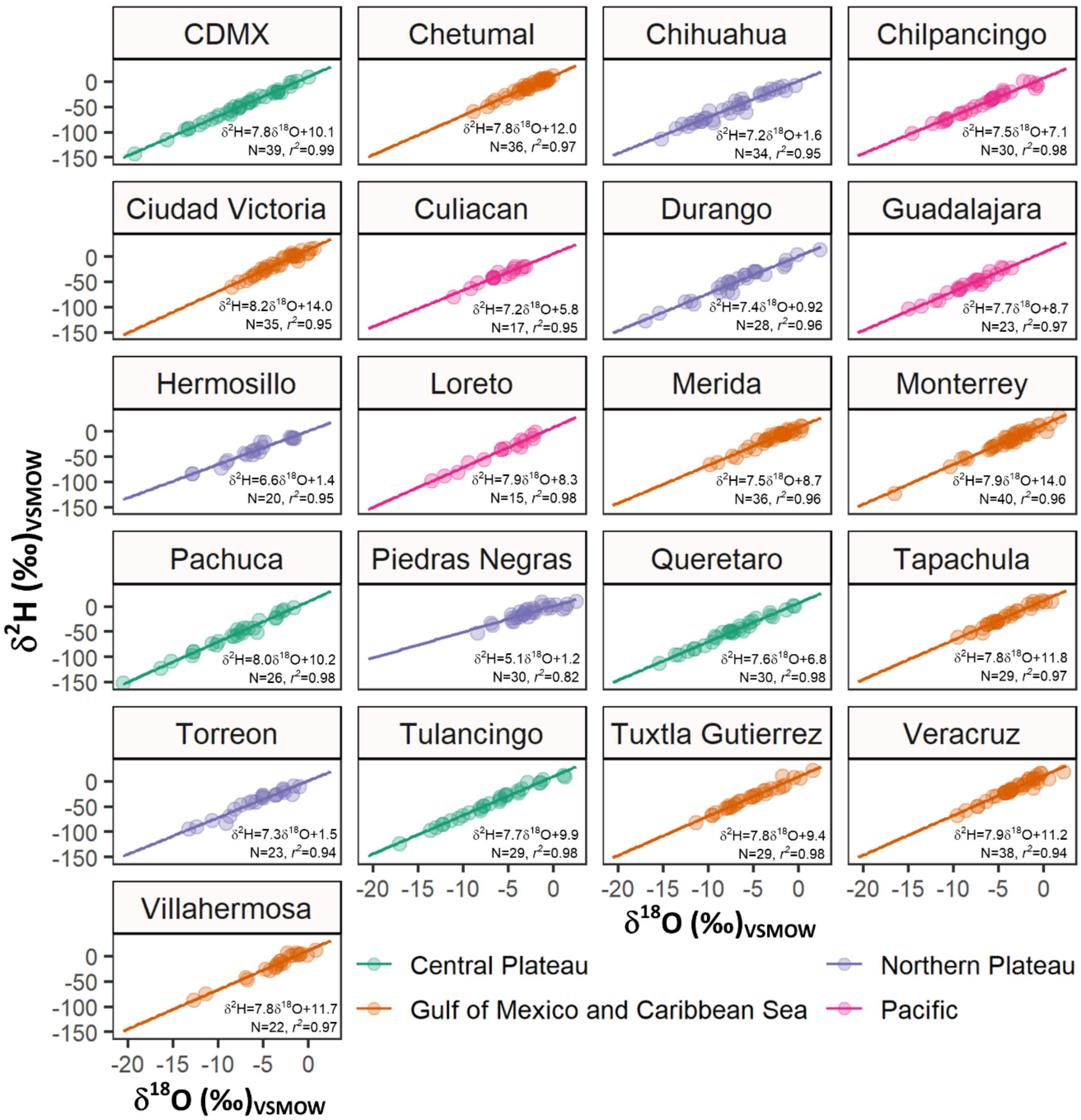

Figure 6: Local meteoric water lines across Mexico between 2018-2021. Regions are color-coded.

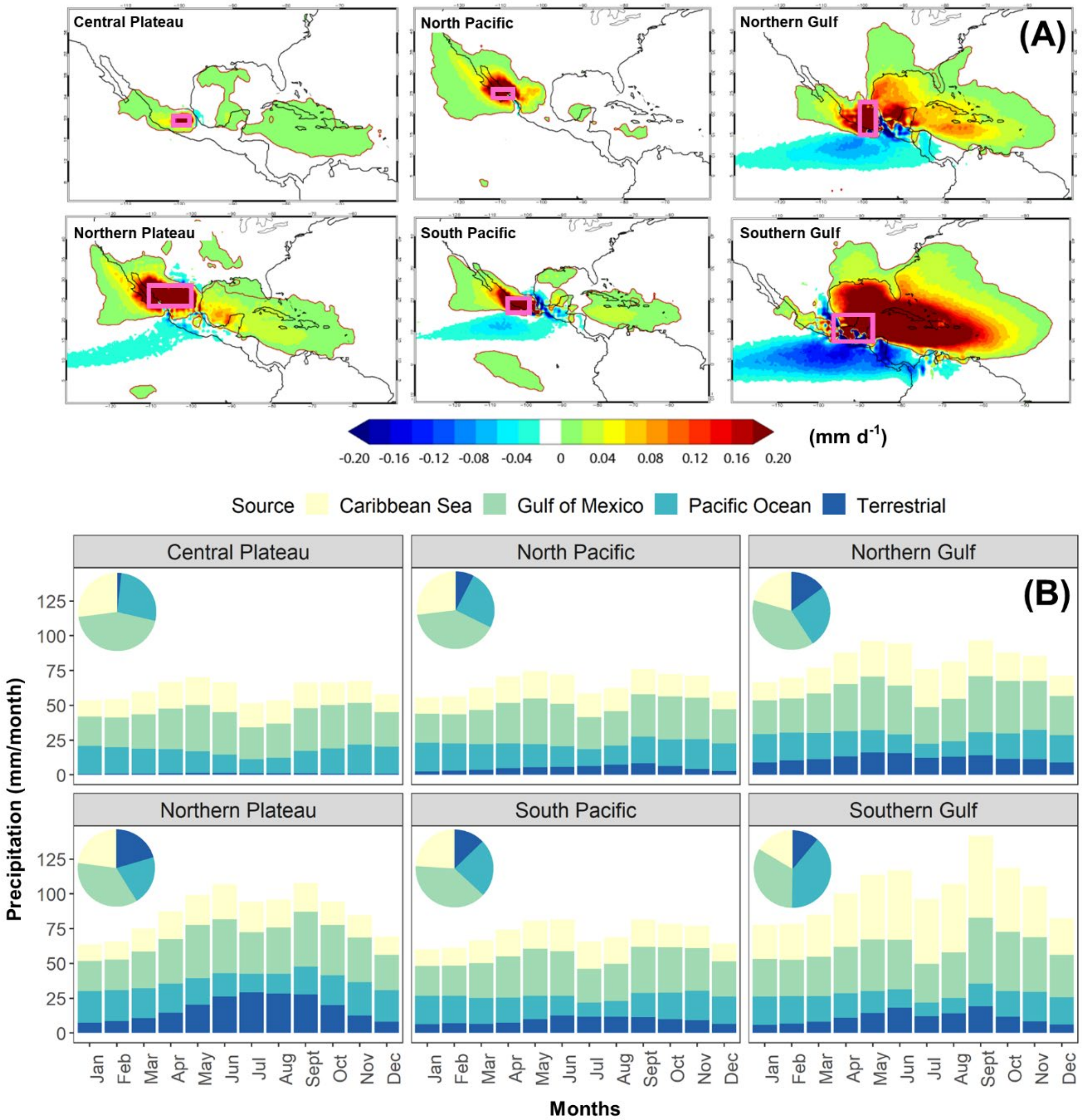

Figure 7: Atmospheric moisture source-sink analysis: A) Spatial distribution of annual moisture source (E-P>0) (in mm d^{-1}) for the study regions (pink polygons). Red areas denote moisture sources. B) Climatological annual cycle of precipitation (mm/month) per region: i) Central Plateau, ii) North Pacific coast, iii) Northern Gulf coast, iv) Northern Plateau, v) South Pacific coast, and vi) Southern Gulf coast. Moisture sources are color-coded: Caribbean basin (yellow), Gulf of Mexico (green), Pacific Ocean (cyan), and terrestrial (blue). The pie charts show the moisture source contribution to the annual precipitation cycle. Period of study: 1980-2018.

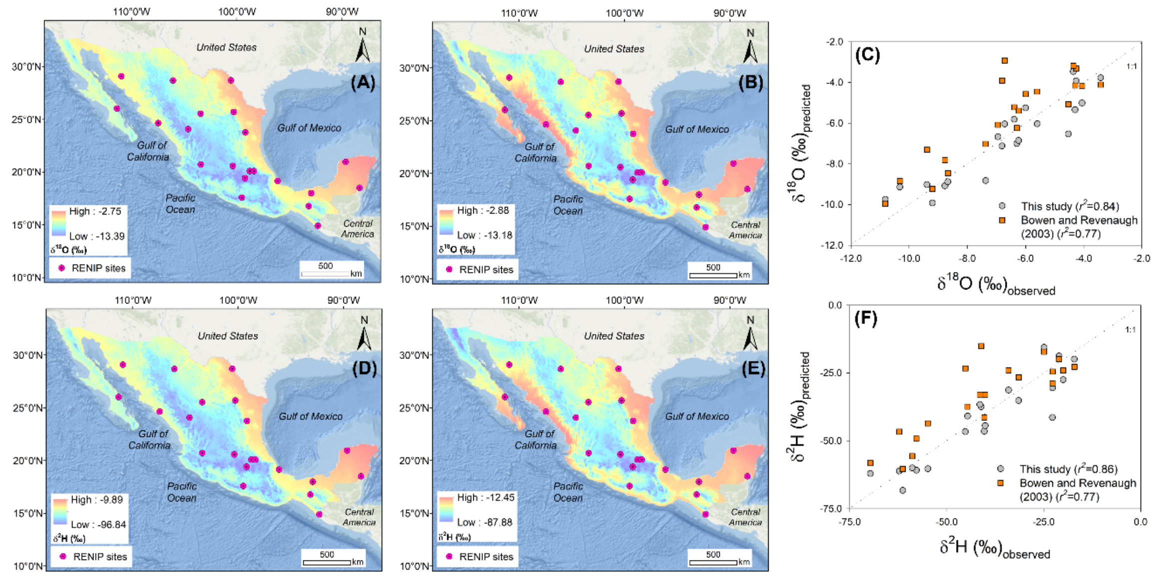

Figure 8: Mean annual isoscape models for δ^{18}O and δ^2H (this study; A and D) versus a global product (B and E) from [54]. Panels C and F show the goodness-of-fit between observed (precipitation-weighted) and predicted δ^{18}O/δ^2H values. Isoscape models based on topographic (elevation) and geographical predictors (latitude and longitude) (orange squares) resulted in an overall improvement (δ^{18}O; *Adj.* r^2=0.84 and δ^2H; *Adj.* r^2=0.86) when compared to global products (gray-dots) based on absolute latitude and elevation (i.e., temperature-driven effects) regressors.

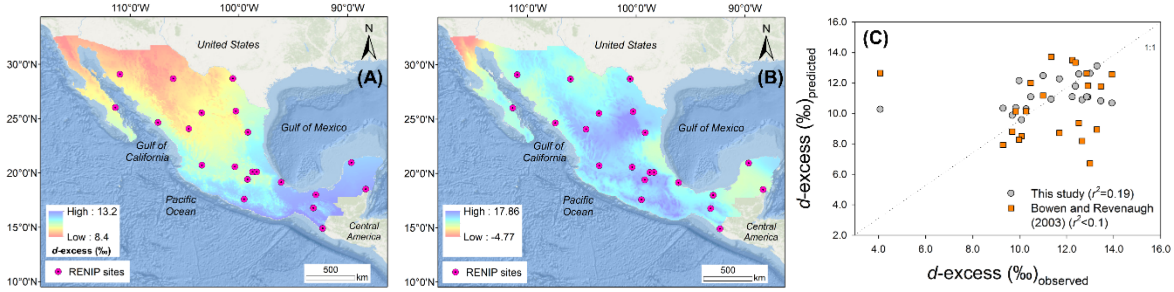

Figure 9: Mean annual isoscape model for *d*-excess (this study; A) versus a global product (B) from [54]. Panel C shows the goodness-of-fit between observed (precipitation-weighted) and predicted *d*-excess values. Both models exhibited poor performance when compared to precipitation-weighted *d*-excess values across Mexico.

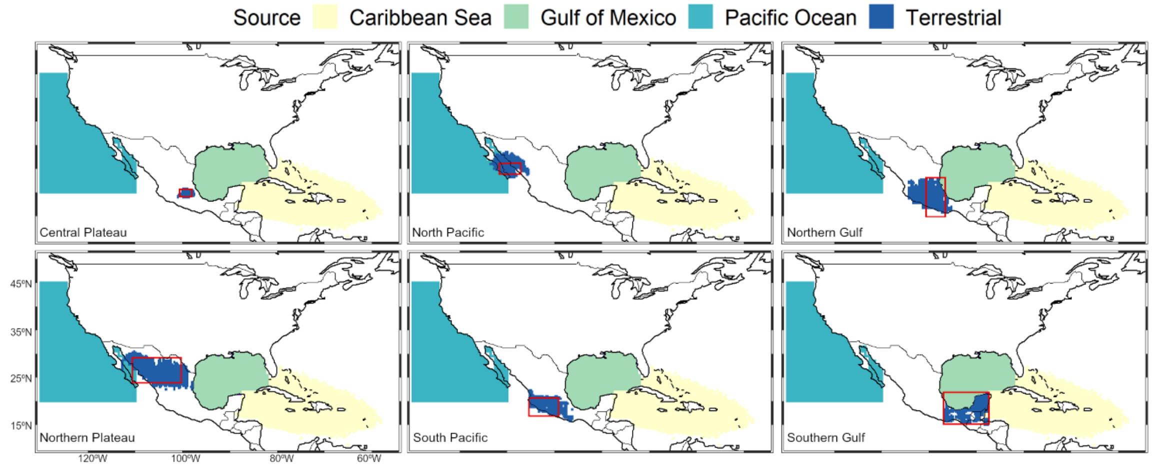

Figure S1: Regional source of atmospheric moisture considered in the experimental setting for the FLEXPART model. Source regions: Pacific Ocean, Gulf of Mexico, Caribbean Sea, and Terrestrial. The red polygons denote the sink regions according to the spatial distribution of the isotope monitoring stations presented in Figure 1.